Title: Lynx1 modulates the activity of nAChRs to slow NMJ and muscle fiber degeneration during aging

Sydney K. Vaughan[1,2], Sebastian Barbat-Artigas[4], Tracey Myers[3], Bhola Shankar Pradhan[5], Tomasz J. Prószyński[5,6], Richard Robitaille[4], Gregorio Valdez[1]

[1] Department of Molecular Biology, Cellular Biology, and Biochemistry, Brown University, Providence, Rhode Island, USA.

[2] Graduate Program in Translational Biology, Medicine, and Health, Virginia Tech, Blacksburg, Virginia, USA.

[3] Fralin Biomedical Research Institute, Roanoke, Virginia, USA.

[4] Département de neurosciences, Université de Montréal, Montréal, QC, Canada.

[5] Laboratory of Synaptogenesis, Nencki Institute of Experimental Biology, Polish Academy of Sciences, Warsaw, Poland.

[6] Laboratory of Synaptogenesis, Łukasiewicz Research Network − PORT Polish Center for Technology Development, Wrocław, Poland

Corresponding Author: Gregorio Valdez

Department of Molecular Biology, Cellular Biology, and Biochemistry

Brown University

70 Ship Street, Providence, RI, 02903

Email: Gregorio_Valdez@brown.edu

Keywords: development, plasticity, cholinergic transmission, aging, miniature endplate potential

Abstract

Cholinergic transmission must be tightly regulated at mammalian neuromuscular junctions (NMJs) for motor neurons and skeletal muscles to properly communicate and remain viable. Here, we examined the function of Lynx1, and endogenous regulator of cholinergic transmission, at NMJs in mice. We show that Lynx1 interacts with and modulates the activity of muscle nicotinic acetylcholine receptors (nAChRs) at NMJs. We also demonstrate that deletion of Lynx1 prematurely and progressively increases the incidence of NMJs with age-related features including fragmentation, nerve sprouting, and multiple innervation. Deleterious changes at NMJs lacking Lynx1 ultimately culminate in the atrophy and de-differentiation of muscle fibers from a fast to a slow phenotype, two hallmarks of aged skeletal muscles. Additionally, we show that Lynx1 is markedly reduced at aged NMJs of control mice, further indicating that Lynx1 plays important roles in mitigating age-related changes at NMJs. These data show that Lynx1 is an attractive target for preventing aging of NMJs and skeletal muscles.

Introduction

Neurotransmission is vital for proper communication across synapses in the central and peripheral nervous systems, and thus normal cognitive and motor functions[1]. In the somatic motor system, cholinergic transmission initiates all voluntary movements. This occurs at the synapse between motor neurons and skeletal muscles, called the neuromuscular junction (NMJ), where acetylcholine (ACh) released from motor axons binds to nicotinic acetylcholine receptors (nAChRs) on skeletal muscles and drives muscle contraction. Because of this critical role in voluntary movement, the cholinergic system is tightly regulated to ensure the proper development, function, and viability of skeletal muscles. For example, the composition and function of nAChRs pentamers changes during development, and in response to conditions that affect the availability of ACh[2]. As NMJs mature, the γ subunit of nAChRs is gradually replaced by the ε subunit[3–5]. The presence of the ε subunit reduces the open time of nAChRs, when bound to ACh, and therefore attenuates their activity. This transition, from nAChRs containing γ to ε subunits, is important for the normal development and function of adult NMJs, and thus skeletal muscles[6]. Highlighting this point, mutations in the ε subunit causes congenital myasthenic syndrome (CMS)[7–12], a neuromuscular disease characterized by muscle weakness and fatigue. The stability and function of adult nAChR pentamers has also been shown to depend on proper phosphorylation of its subunits and on associations with other key molecules involved in nAChR trafficking, clustering, and anchoring[13–18]. Thus, multiple mechanisms have been found to alter the properties of nAChRs to regulate the response of muscle fibers to changes in cholinergic transmission.

59 Evidence continues to accumulate indicating that changes in the cholinergic
60 system may contribute to NMJ degeneration and muscle fiber atrophy[19–21]. In skeletal
61 muscles of old animals and afflicted with amyotrophic lateral sclerosis (ALS), the γ subunit
62 is elevated compared to muscles in healthy young adult mice[22,23]. There is also evidence
63 indicating that presynaptic sites fail to adequately control the release of ACh in aged and
64 ALS affected animals[24–26]. ACh acts as an anti-synaptogenic factor by directly promoting
65 the disassembly of nAChR clusters[14], in addition to its classical role as a neurotransmitter.
66 Through this action, a moderate yet consistent increased in the release of ACh from the
67 random fusion of synaptic vesicles may destabilize nAChR clusters and thereby
68 contribute to degeneration of NMJs during aging and in ALS. Supporting this possibility,
69 we recently demonstrated that NMJs prematurely acquire age-associated features in
70 transgenic mice which have increased levels of ACh in synaptic vesicles[27]. These
71 published findings strongly suggest that aberrant cholinergic transmission may promote
72 degeneration of adult NMJs and muscle fibers.

73 Although years of efforts have revealed the identity of many critical components of
74 the cholinergic system at NMJs, it remains unknown if Lynx1 is present and modulates
75 nAChRs at NMJs. Lynx1 is a GPI-anchored protein present on the cell surface shown to
76 interact with and modulate the function of nAChRs in the central nervous system (CNS)[28–
77 31]. In the brain, Lynx1 has been shown to modulate the activity of α7 and $\alpha_2\beta_4$
78 pentamers[30–32]. Lynx1 has also been found to inhibit neuronal plasticity in the visual and
79 auditory cortex by reducing the sensitivity of nAChRs to ACh[33–35]. Additionally, there is
80 evidence that while loss of Lynx1 augments motor learning during normal aging, it also
81 contributes to neuronal degeneration in the dorsal striatum[36,37]. We therefore

82 hypothesized that Lynx1 is present and modulates the activity of muscle specific nAChR
83 pentamers at NMJs.

84 We carried out complementary experiments to examine the function of Lynx1 in
85 skeletal muscles, specifically at NMJs. We discovered that Lynx1 is indeed expressed in
86 skeletal muscles and progressively concentrates at NMJs during development.
87 Importantly, we show that Lynx1 interacts with and modulates the activity of nAChRs at
88 the NMJ. We also found that while loss of Lynx1 does not affect developing NMJs, it
89 accelerates the appearance of age-related features at NMJs in young adult and middle-
90 aged mice. Furthermore, the deleterious changes at NMJs resulting from loss of Lynx1
91 ultimately cause muscle atrophy in adult mice. Consistent with these data from knockout
92 mice, we found that Lynx1 is significantly decreased at aged NMJs of control mice.
93 Together, these data show that Lynx1 modulation of nAChRs is important for the
94 maintenance of NMJs and viability of muscle fibers.

95 **Results**

96 ***Muscles fibers express and concentrate Lynx1 in the postsynaptic region***

97 We first sought to determine if Lynx1 is expressed in skeletal muscles, and
98 specifically by muscle fibers. We examined Lynx1 transcripts in ribosomal mRNA
99 fractions specifically isolated from fast-type muscle fibers within the tibialis anterior (TA)
100 muscle. We accomplished this by crossing mice expressing the ribosomal protein Rpl22
101 tagged with HA epitopes[38] (RiboTag$^{flox/flox}$) with parvalbumin-Cre (PVCre) transgenic
102 mice[39] to generate PVCre; RiboTag$^{flox/flox}$ offspring. HA-tagged Rpl22 is expressed in fast-
103 type muscle fibers, which constitute the majority of muscle fibers in the TA muscle, in
104 PVCre; RiboTag$^{flox/flox}$ mice. This approach revealed that Lynx1 transcripts are enriched

105 in ribosomal mRNA fractions obtained from the TA muscle compared with total muscle
106 mRNA. (Fig. 1A). We then examined the temporal expression of Lynx1 in skeletal
107 muscles of wild-type mice. We found that Lynx1 transcripts increase in the TA muscle as
108 mice transition from postnatal to the juvenile stage of life (Fig. 1B). We validated these
109 findings in C2C12-derived myotubes, which increase expression of Lynx1 as they mature
110 (Fig. 1C). Importantly, we immunostained skeletal muscles for Lynx1 and found Lynx1
111 localized at the NMJ, based on staining of nAChRs using fluorescently tagged α-
112 bungarotoxin (BTX) (Figure 1D-E). This analysis also showed that Lynx1 protein gradually
113 increases and specifically at NMJs during development (Fig. 1F). Thus, muscle fibers
114 express and concentrate Lynx1 in the postsynaptic region of the NMJ.

115 **Lynx1 interacts with nAChRs of the NMJ**

116 The findings above, along with published data[28,30–32,40,41], suggest that Lynx1
117 accumulates in the postsynaptic region of the NMJ to interact with and modulate the
118 activity of nAChRs. To test the first possibility, we performed a series of biochemical
119 experiments. To start, we used homogenates from HEK293 cells co-transfected with
120 mCherry-tagged Lynx1 and four different muscle nAChR subunits (alpha, beta, delta, and
121 epsilon). Because these four subunits assemble at the peripheral membrane, this co-
122 transfection strategy allowed us to test the interaction between Lynx1 and nAChR
123 pentamers. Following immunoprecipitation with a pan-antibody against the nAChR
124 pentamer and western blotting, we found that Lynx1, revealed using an antibody against
125 mCherry, is only pulled down from cells co-transfected with the nAChR subunits (Fig. 2A).
126 We then asked if Lynx1 interacts with a specific subunit of the nAChR pentamer. For this,
127 we generated recombinant alpha, beta, delta, epsilon, and gamma nAChR subunits

128 tagged with glutathione S-transferase (GST). We used these recombinant proteins to coat
129 GST beads to precipitate mCherry-Lynx1 from HEK293 lysates. As shown in figure 2B,
130 all nAChR subunits precipitated Lynx1 fusion protein, indicating that Lynx1 may bind to
131 each nAChR subunit. Finally, and most importantly, we asked if the interaction between
132 nAChRs and Lynx1 is direct or indirect. We performed classical pull-down experiments
133 after incubating purified GST-Lynx1 with the ectodomain of the alpha subunit also tagged
134 with GST. In this case, the GST-tagged alpha subunit was pulled-down with bungarotoxin
135 coated beads. We again found that Lynx1 co-precipitates with the alpha subunit revealed
136 by Western blot with anti-GST antibody (Fig. 2C). To validate this finding, we purified and
137 incubated 6-His-Lynx1 with the extracellular portions of each nAChR subunit, alpha, beta,
138 delta, epsilon, and gamma, tagged with GST. We then immunoprecipitated the nAChR
139 subunits using anti-GST coated beads. As shown in figure 2D, each nAChR subunit co-
140 precipitated 6-His-Lynx. Collectively, these experiments strongly indicate that Lynx1
141 directly interacts with all the nAChR subunits.

142 ***Lynx1 modulates the sensitivity of nAChR to ACh in skeletal muscles***

143 The association between Lynx1 and nAChRs in skeletal muscles suggests that
144 Lynx1 functions to regulate cholinergic activity at the NMJ. To determine the function of
145 Lynx1 at the NMJ, we first examined miniature endplate potentials (MEPPs), as they
146 directly reflect properties of postsynaptic receptors. Using NMJs from 4-month-old Lynx1^{-}
147 $^{/-}$ mice and controls (Fig. 3A-B), we observed that the mean amplitude and frequency of
148 MEPPs are unchanged in NMJs lacking Lynx1 (Fig. 3C-D). However, the rise time, which
149 reflects the binding of ACh to its receptors, was significantly faster in Lynx1$^{-/-}$ NMJs
150 compared to controls (Control=1.33±0.0952ms; Lynx1$^{-/-}$=0.857±0.1321ms, p=1.66E-27;

151 Fig. 3E). Supporting this finding, the slope to reach the maximum MEPP amplitude is
152 steeper at NMJs lacking Lynx1 (Fig. 3F). However, loss of Lynx1 does not alter the EPP
153 amplitude (Fig. 4A-B), or the quantal content (Fig. 4C) at NMJs. These data indicate that
154 while the binding of nAChRs to ACh and the postsynaptic response was facilitated, the
155 probability of ACh release remains unaltered at NMJs in Lynx1$^{-/-}$ mice.

156 We next asked if synaptic plasticity events elicited by sustained motor nerve
157 stimulation (120 Hz, 10 s) were altered in NMJs lacking Lynx1. At NMJs of control mice,
158 we observed a rapid and short-lasting depression (74.96±1.589%; Fig. 4D) that was
159 followed by a delayed, long-lasting depression (11.88±3.635%; Fig. 4D). However, in
160 NMJs of Lynx1$^{-/-}$ mice, while the rapid and short-lasting synaptic depression was
161 unchanged (77.74±1.553%; Fig. 4D), we observed a significant post-tetanic potentiation
162 (12.22±3.688%) and the delayed, long-lasting depression, was obliterated (Fig. 4D).

163 We also tested the possibility that altered synaptic properties in Lynx1$^{-/-}$ NMJs may
164 lead to changes in muscle function. We used a force transducer to measure the contractile
165 properties of the EDL muscle following either direct muscle stimulations or nerve-evoked
166 synaptic activity to elicit contractions. We found that muscles lacking Lynx1 generated
167 less force when stimulated directly (Control=59.16±2.243%; Lynx1$^{-/-}$=47.15±3.831%,
168 p=0.0186 at 1min; Fig. 4E), whereas responses remained the same when nerve-evoked.
169 This data shows that loss of Lynx1 compromises the function of skeletal muscles.

170 ***Lynx1 is not required at NMJs and muscle fibers during development***

171 We found that Lynx1 expression and localization at NMJs progressively increases
172 as muscle fibers mature (Fig. 1). These findings suggested that Lynx1 may play roles in
173 the maturation and stability of NMJs and muscle fibers. To start looking into this

174 possibility, we examined the impact of deleting Lynx1 on developing NMJs and muscle
175 fibers in the EDL and soleus muscles of postnatal day 6 (P6) mice. This is an age when
176 NMJs and muscle fibers are undergoing fast and dramatic morphological, molecular, and
177 functional changes in mice[42]. This analysis showed no significant morphological
178 differences in NMJs and muscle fibers between control and Lynx1$^{-/-}$ mice (Supplementary
179 Figure 1A-J). Furthermore, there were no differences in levels of the α, β, δ, ε, or γ nAChR
180 subunits in Lynx1$^{-/-}$ mice compared to control mice (Supplementary Figure 1K). Similarly,
181 the expression of acetylcholinesterase (AChE), Muscle-Specific Kinase (MuSK), Low-
182 density lipoprotein receptor-related protein 4 (LRP4), and Receptor-Associated Protein of
183 the Synapse (Rapsyn) remained unchanged in Lynx1$^{-/-}$ mice compared to control mice at
184 P6 (Supplementary Figure 1L-O). Together, these findings show that Lynx1 is not
185 required for the proper cellular and molecular maturation of the NMJ.

186 To determine if the loss of Lynx1 affects the maturation of muscle fibers, we
187 analyzed TA muscles from P6 Lynx1$^{-/-}$ and control mice. As expected, based on our
188 analysis of NMJs, there were no significant differences in the average muscle fiber area
189 or frequency distribution of muscle fiber areas in Lynx1$^{-/-}$ mice compared to controls
190 (Supplementary Figure 2A-D). The incidence of muscle fibers with centralized nuclei, a
191 proxy for immature and also regenerating muscle fibers, is unchanged at P6 in mice
192 lacking Lynx1 compared to age-matched control mice (Supplementary Figure 2E).
193 Molecularly, there were no significant differences in the expression profile of myosin
194 heavy chains I, IIa, IIb, and IIx in Lynx1$^{-/-}$ mice compared to control mice (Supplementary
195 Figure 2F). The loss of Lynx1 also did not impact the expression of two pro-myogenic

196 genes, Pax7[43] or myogenin[44] (Supplementary Figure 2G-H). Taken together, these data
197 show that Lynx1 is not required for the proper and timely maturation of muscle fibers.

198 ***Lynx1 functions to stabilize the NMJ***

199 Lynx1 concentration is highest at adult NMJ (Fig. 1) where it modulates the activity
200 of nAChRs (Fig. 3, Fig. 4). To further discern the role of Lynx1 in skeletal muscles, we
201 then examined the impact of deleting Lynx1 on adult NMJs in the EDL muscles of 4-
202 month-old mice. This analysis revealed several structural differences at NMJs of Lynx1$^{-/-}$
203 compared to control mice (Fig. 5A-B). These included a significant increase in the number
204 of denervated and fragmented NMJs in Lynx1$^{-/-}$ compared to control mice (Fig. 5C). Even
205 though the size of the NMJ was unchanged (Fig. 5D), there was a marked reduction in
206 the density of nAChRs in the postsynaptic region in Lynx1$^{-/-}$ compared to control mice
207 (Fig. 5E). Additionally, adult Lynx1$^{-/-}$ mice had more motor axons with large blebs proximal
208 to the NMJ (Fig. 5F). Despite these changes, muscle fibers remained largely singly
209 innervated in in Lynx1$^{-/-}$ compared to control mice (Fig. 5F). Because of these findings,
210 we were not surprised to find transcripts for each nAChR subunit, MuSK, and LRP4
211 significantly elevated in skeletal muscles lacking Lynx1 (Fig. 5G-I). However, Rapsyn was
212 decreased in Lynx1$^{-/-}$ mice (Fig. 5J). These data support immunohistochemical analysis
213 showing reduced intensity of nAChRs at NMJs lacking Lynx1 (Fig. 5E) for two reasons.
214 First, it has been shown that nAChR subunits, MuSK and LRP4 are increased to
215 compensate for loss of nAChR pentamers[45]. Second, the decreased expression of
216 Rapsyn, which anchors nAChR clusters to the plasma membrane in a 1:1 stoichiometry[46],
217 demonstrates that nAChR pentamers are unstable and likely turnover at a faster rate in
218 muscles lacking Lynx1. Additionally, we found acetylcholinesterase (AChE) increased in

219 Lynx1$^{-/-}$ mice (Fig. 5K). As shown below, we hypothesize that muscle fibers lacking Lynx1
220 increase levels of AChE because of augmented sensitivity of nAChRs to ACh, and not as
221 a result of higher levels of ACh at the synaptic cleft. Altogether, these findings
222 demonstrate that Lynx1 plays important roles at adult NMJs.

223 Based on the above findings, we hypothesized that NMJs lacking Lynx1 would
224 continue to accrue age-related features at a faster rate with advancing age. To test this
225 hypothesis, we extended our analysis to middle-aged, 12-month-old, mice (Fig. 6A-B).
226 We again found a higher incidence of denervated and fragmented NMJs in middle-aged
227 Lynx1$^{-/-}$ mice compared to age- and sex-matched control mice (Fig. 6C). Middle-aged
228 Lynx1$^{-/-}$ mice also presented with smaller receptor area (Fig. 6D) and reduced nAChRs
229 density, revealed by the lower intensity of BTX (Fig. 6E). Additionally, middle-aged Lynx1^{-}
230 $^{/-}$ mice had more multiply innervated NMJs and innervating motor axons with large blebs,
231 a hallmark of degenerating axons (Fig. 6F). This data showed that NMJs lacking Lynx1
232 accrue additional age-related features. To complement this cellular data, we again
233 examine expression of genes critical for the stability and function of the NMJ. We found
234 most nAChR subunits expressed at lower levels in middle-aged Lynx1$^{-/-}$ mice compared
235 to age-matched control mice (Fig. 6G). Interestingly, these expression patterns of nAChR
236 subunits are in contrast to those of young adult mice (Figure 5G). MuSK, LRP4, and
237 Rapsyn were unchanged in middle-aged Lynx1$^{-/-}$ mice compared to age-matched control
238 mice (Fig. 6H-J). AChE was found decreased in middle-aged Lynx1$^{-/-}$ mice compared to
239 age-matched control mice (Fig. 6K). These findings suggest that skeletal muscles lacking
240 Lynx1 prematurely lose the capacity to recruit compensatory mechanisms important for
241 stabilizing and repairing damages at NMJs with advancing age.

242 ***Increased nAChR turnover in Lynx1 null mice***

243 In mice lacking Lynx1, there is a marked reduction in the density of nAChRs at
244 NMJs. Since Lynx1 binds to these receptors, it raised the possibility that Lynx1 also
245 functions to stabilize nAChRs at the membrane. To test this possibility, we examined the
246 rate of nAChRs turnover in the sternomastoid muscle of 3-month-old Lynx1$^{-/-}$ and control
247 mice following in vivo labeling with saturating levels of alexa-488 conjugated BTX (A488-
248 BTX). We then used alexa-555 conjugated BTX (A555-BTX) to reveal newly inserted
249 nAChRs at NMJs[47] (Fig. 7A-C). Demonstrating the validity of this approach, A555-BTX
250 failed to label NMJs in the sternomastoid when it was fixed immediately following
251 exposure to saturating concentrations of A488-BTX (Supplementary Figure 3). We
252 analyzed the intensity profile of alexa-488 and alexa-555 labeled nAChRs to determine
253 the ratio of new to old nAChRs across the endplate region (Fig. 7D-E). In the
254 sternomastoid of Lynx1$^{-/-}$ mice, the average ratio of new to old nAChRs at NMJs was
255 significantly higher compared to control mice (Fig. 7F). During the course of this
256 experiment, we observed considerable variability in A555-BTX staining among NMJs
257 within sternomastoid muscles from the same animal. We attributed this variability to
258 differences in nAChR turnover rates due to varied functional demands on NMJs within
259 the same muscle. To account for this variability across NMJs, we examined the frequency
260 of NMJs with specific ratios of new to old nAChRs. We again found significantly more
261 NMJs with a higher ratio of A555-BTX to A488-BTX, and thus newer nAChRs, in Lynx1$^{-/-}$
262 mice (Fig. 7G). These data show that Lynx1 functions to stabilize nAChRs at NMJs in
263 addition to modulating their sensitivity to ACh.

264 ***Muscle atrophy follows deleterious changes at NMJs in mice lacking Lynx1***

265 Even though Lynx1 concentrates and modulates the function of nAChRs at NMJs,
266 it is plausible that NMJs lacking Lynx1 accrue deleterious features resulting from changes
267 elsewhere in muscle fibers or motor neurons. To address this possibility, we first
268 examined muscle fibers for signs of atrophy and turnover in 4- and 12-month-old mice
269 with and without Lynx1. To compare changes in muscle size between genotypes and thus
270 determine if deletion of Lynx1 causes atrophy, we measured the cross-sectional area
271 (CSA) of individual muscle fibers and the whole TA muscle. We used the same samples
272 to determine the location of myonuclei, with those located away from the peripheral
273 membrane indicating that the muscle fiber had degenerated and regenerated. This
274 analysis revealed no difference in the average muscle fiber CSA (Supplementary Figure
275 4A-C) and in the CSA frequency distribution of individual muscle fibers between 4-month-
276 old Lynx1$^{-/-}$ and control mice (Supplementary Figure 4D). The CSA of the whole TA
277 muscle was also unchanged in 4-month-old Lynx1$^{-/-}$ compared to control (Supplementary
278 Figure 4E). Similarly, the occurrence of centralized myonuclei was unchanged in young
279 adult Lynx1$^{-/-}$ (Supplementary Figure 4F). Hence, we found no obvious signs of muscle
280 fiber atrophy in mice lacking Lynx1 at 4 months of age even though NMJs have clearly
281 begun to degenerate at this age (Fig. 5).

282 We also examined the expression of genes associated with the formation, health
283 and identity of muscle fibers. There was a significant reduction of Pax7 and myogenin
284 levels in Lynx1$^{-/-}$ compared to control mice (Supplementary Figure 4G, H), two genes
285 important for myogenesis. Additionally, we found a marked increase in levels of atrogin-
286 1 and Forkhead Box O1 (FOXO-1), which promote muscle atrophy, in 4-month-old Lynx1^{-}

287 $^{/-}$ mice compared to age-matched control mice (Supplementary Figure 4I, J). As
288 previously shown[19,21], these molecular alterations may be driven by dysregulated
289 cholinergic transmission at NMJs resulting from loss of Lynx1. However, the loss of Lynx1
290 had no effect on levels of myosin heavy chains I, IIa, IIb, and IIx in the TA muscle at 4
291 months of age (Supplementary Figure 4K).

292 Since NMJs continue to degenerate with advancing age in mice lacking Lynx1, we
293 surmised that muscle fibers would ultimately atrophy and exhibit signs of regeneration in
294 older mice. Indeed, the average muscle fiber CSA was significantly reduced in 12-month-
295 old Lynx1$^{-/-}$ mice compared to age- and sex-matched control mice (Fig. 8A-C). In the TA
296 muscle of Lynx1$^{-/-}$ mice, the overall size reduction resulted from the presence of more
297 muscle fibers with a reduced CSA, revealed using a cumulative frequency histogram plot
298 (Fig. 8D). Not surprisingly, the CSA of the whole TA muscle was significantly smaller in
299 12-month-old Lynx1$^{-/-}$ compared to control (Fig. 8E). Supporting these findings, muscle
300 fibers lacking Lynx1 were populated with more centralized myonuclei (Fig. 8F).
301 Additionally, we found that Pax7 was significantly reduced in the TA muscle of middle-
302 aged Lynx1$^{-/-}$ mice compared to controls of the same age (Fig. 8G). However, myogenin
303 was increased (Fig. 8H) while atrogin-1 was unchanged, and FOXO-1 was reduced in 12-
304 month-old Lynx1$^{-/-}$ mice compared to control mice (Fig. 8I, J).

305 In addition to muscle atrophy, aging causes fast-type muscle fibers to de-
306 differentiate into slow types[48–50]. To determine if this shift occurs prematurely in mice
307 lacking Lynx1, we visualized muscle fiber types using antibodies against MYHCIIa and
308 MYHCIIb (Fig. 9A-C). We found fewer MYHCIIb-positive muscle fibers and more muscle
309 fibers that were either MYHCI or MYHCIIx in Lynx1$^{-/-}$ mice (Fig. 9D). To corroborate these

310 findings, we assessed transcript levels for each myosin heavy chain and found a
311 significant increase in MYHCI expression in Lynx1$^{-/-}$ muscles compared to age-matched
312 controls (Fig. 9E). These data show that loss of Lynx1 affects the identity, and importantly
313 the viability of muscle fibers. However, these myogenic changes occur after NMJs lacking
314 Lynx1 have accrued significant functional and structural deleterious features (Fig. 5).

315 ***Motor neurons do not atrophy in Lynx1$^{-/-}$ mice***

316 Lynx1 was found to be expressed in the ventral horn of the spinal cord[51], where
317 motor neurons reside. This raised the possibility that global deletion of Lynx1 may also
318 compromise the function and health of motor neurons. In this case, the changes observed
319 at NMJs of mice lacking Lynx1 may result from alterations in motor neurons. However,
320 we found no difference in the size of motor neurons between Lynx1$^{-/-}$ and control mice at
321 4 and at 12 months of age (Supplementary Figure 5). This finding along with
322 electrophysiological recordings indicating normal EPP, a readout of presynaptic function,
323 indicate that global deletion of Lynx1 does not alter the viability and function of motor
324 neurons. Moreover, these data further indicate that deletion of Lynx1 causes pathological
325 changes first at NMJs, which then compromises the viability of skeletal muscles.

326 ***Lynx1 is reduced at aged NMJs***

327 Finally, we asked if aberrant changes in Lynx1 may contribute to the inevitable
328 degeneration of NMJs that occurs with advancing age in control mice. We compared
329 Lynx1 distribution and expression between old and young NMJs. Immunostaining and
330 light microscopy analysis showed that Lynx1 is markedly reduced in NMJs of 24-month-
331 old compared to 4-month-old mice (Fig. 10A-C). The loss of Lynx1 from aged NMJs does
332 not result from decreased expression since its transcripts were found expressed at similar

333 levels in the TA muscle of old and young mice (Fig. 10D). The decreased concentration
334 of Lynx1 at aged NMJs was also uncorrelated with changes in expression of most nAChR
335 subunits, as most were increased in aged compared to young skeletal muscles (Fig. 10E).
336 This finding mirrors the expression pattern of nAChRs in 4-month-old mice lacking Lynx1.
337 Thus, the loss of endogenous Lynx1 from aging NMJs may contribute to the instability of
338 nAChRs and thereby age-related neuromuscular degeneration.

339 **Discussion**

340 Lynx1, an endogenous regulator of cholinergic activity, was first described in 1999
341 in the brain[28]. Initial reports revealed structural similarities between Lynx1 and α-
342 bungarotoxin, which binds with high affinity to nAChRs. The GPI anchor, which attaches
343 Lynx1 to the membrane[28], primarily distinguishes Lynx1 from α-bungarotoxin and other
344 neurotoxins. Further analysis confirmed that Lynx1 interacts with nAChRs and functions
345 to maintain a low sensitivity to ACh, contributing to the synaptic safety margin[31]. In
346 addition to interacting with nAChRs on the peripheral membrane, Lynx1 binds to nAChRs
347 in the endoplasmic reticulum where it shifts the stoichiometry of subunits to generate a
348 nAChR pentamer with lower sensitivity to ACh[32]. This interaction within the endoplasmic
349 reticulum has been suggested to be mediated through the preferential binding of Lynx1
350 to specific subunit interfaces[30]. Analysis of Lynx1 knockout mice has provided valuable
351 insights into its role in vivo. Lynx1 was found to be an allosteric modulator of nAChRs,
352 critical for neuronal survival[40]. More recently, Lynx1 has been implicated in neuronal
353 plasticity[34,35,52], motor learning[37], aging[36], Alzheimer's[53], nociception[54], and nicotine
354 addiction[29].

355 Despite the essential role nAChRs play at NMJs, Lynx1 had yet to be studied in
356 skeletal muscles, and specifically at NMJs. As Dr. Zach Hall eloquently wrote in 1999, “A
357 physiological role for Lynx1 at [the neuromuscular junction] would bring the α neurotoxin
358 story full circle in a historically fitting and entirely satisfying way”[55]. Previous studies using
359 a water-soluble version of Lynx1, which lacks the GPI anchor, found competitive binding
360 between Lynx1 and α-bungarotoxin in AChBP and *T. californica* nAChRs and identified
361 residues responsible for this interaction[41,56]. These data indicated for the first time that
362 Lynx1 could potentially interact with muscle nAChRs. However, many questions remained
363 regarding Lynx1 at NMJs. This included whether Lynx1 interacts with and modulates the
364 activity of mammalian nAChRs and the biological significance of this function on the
365 maintenance and stability of NMJs.

366 This study examined the role of Lynx1 in skeletal muscles, and particularly at NMJs
367 in mice. We show that Lynx1 expression increases and concentrates at NMJs during
368 development. We also demonstrate that Lynx1 vacates NMJs with advancing age.
369 Importantly, we provide data revealing the function of Lynx1 at the NMJ. We demonstrate
370 that Lynx1 interacts with nAChRs to impact synaptic and muscle properties. It also
371 functions to stabilize nAChRs at the NMJ. Additionally, we show that Lynx1 plays a critical
372 role in slowing the appearance of age-related pathological features in NMJs that
373 culminate in the atrophy of muscle fibers. Thus, this study demonstrates that Lynx1
374 modulates the activity of nAChRs to preserve the function and structure of NMJs and
375 muscle fibers.

376 We found that Lynx1 progressively increases when significant morphological and
377 functional changes are occurring at maturing NMJs and muscles fibers[42]. However,

378 deletion of Lynx1 did not cause obvious morphological and molecular changes in
379 developing NMJs and muscle fibers. Why then do developing muscle fibers progressively
380 increase the expression of and concentrate Lynx1 at the NMJ? We hypothesize that
381 Lynx1 upregulation may be a preparatory step to ensure that the cholinergic system
382 functions optimally in matured and less plastic NMJs and skeletal muscles. We base this
383 hypothesis on the fact that adult, but not developing, NMJs are susceptible to a rather
384 moderate increase in cholinergic transmission[19]. It is also worth noting that in immature
385 muscles, the presence of the γ subunit potentially negates the further sensitization of
386 nAChRs to ACh caused by loss of Lynx1.

387 The data in this study, however, do support important roles for Lynx1 in maintaining
388 the normal function and stability of adult NMJs by modulating the activity of nAChRs. They
389 are also in line with published findings indicating that aberrant changes in the cholinergic
390 system contribute to aging of the NMJs and skeletal muscles. For example, numerous
391 studies have shown increases in the amplitude and/or frequency of miniature endplate
392 potentials (MEPPs), which represent the random fusion of vesicles at active zones,
393 endplate potentials (EPPs), and spontaneous giant miniature endplate potentials
394 (GMEPPs), which occur when ACh is released from vesicles residing outside the active
395 zone, in various skeletal muscles in old age[26,57–59]. These findings were confirmed in a
396 recent study that compared cholinergic transmission at NMJs of 12-14 month-old versus
397 24-28 month-old mice[60]. Demonstrating that augmented cholinergic transmission
398 contributes to NMJ degeneration, our lab recently showed that a moderate increase in
399 MEPP amplitude resulting from elevated ACh causes NMJs to prematurely acquire age-
400 related morphological features in young adult mice[27]. Thus, the loss of Lynx1 from aged

401 NMJs likely augments the activity of nAChRs, further exacerbating the deleterious effects
402 of dysregulated cholinergic transmission that occurs with advancing age. Given that
403 Lynx1 stabilizes nAChRs at the postsynapse, its loss may also underlie the instability of
404 nAChRs at aged NMJs[17,61–63].

405 While this study unraveled a number of key roles of Lynx1 at NMJs and in skeletal
406 muscles, it also raised a number of additional questions. This includes the identity of
407 molecular mechanisms, influenced by cholinergic activity, that regulates the expression
408 of Lynx1. This study also did not address the underlying reason for the loss of Lynx1 from
409 aged NMJs. Additionally, it remains unknown if the absence of Lynx1 accelerates the
410 turnover of nAChRs at NMJs by causing physical instability, or by changing their
411 phosphorylation status due to increased binding to ACh. Answers to these questions
412 would serve as the basis to preserve and restore the function of Lynx1 along with proper
413 cholinergic transmission. Because of its role in modulating cholinergic transmission,
414 Lynx1 is a promising candidate for mitigating the ravages of aging and other conditions,
415 including ALS, nerve injuries and myasthenia gravis, all of which are known to alter
416 cholinergic transmission and have either negative or positive actions on NMJs and
417 muscles fibers[64–66]. Lynx1 may also confer benefits to muscle recovery following exercise
418 where again cholinergic transmission fluctuates[67]. Thus, future studies should determine
419 the specific role for Lynx1 in different conditions and at specific stages when cholinergic
420 transmission is either heightened or diminished.

421 **Methods**

422 ***Source of mice***

423 We obtained Lynx1$^{-/-}$ mice[40] from the lab of Dr. Morishita and began a colony of our own.
424 These mice were mated with Thy1-YFP16[68] (RRID:IMSR_JAX:003709) animals in our
425 colony to generate Lynx1$^{-/-}$;Thy1-YFP animals. In order to have littermate pairs, Lynx1$^{+/-}$
426 ;Thy1-YFP mice were mated together to yield litters with Lynx1$^{-/-}$;Thy1-YFP and Thy1-
427 YFP control mice. The colony is maintained on a C57BL/6 background. The following
428 mice were obtained from The Jackson Laboratory: Parvalbumin-Cre[39]
429 (RRID:IMSR_JAX:017320), and RiboTag[38] (RRID:IMSR_JAX:011029) and bred to
430 generate PVCre; RiboTag$^{flox/flox}$ offspring. Mice were anesthetized with isoflurane,
431 followed by immediate dissection and collection of fresh tissues, or by transcardial
432 perfusion with 1XPBS (pH 7.4) followed by 4% paraformaldehyde (PFA, pH 7.4) for fixed
433 tissues. All experiments were carried out under the NIH guidelines and animal protocols
434 approved by the Virginia Tech Institutional Animal Care and Use Committee or in
435 accordance with the guidelines of the Canadian Council of Animal Care and the Comité
436 de déontologie animale of Université de Montréal.

437 ***C2C12 cultures***

438 C2C12 cells were plated in 8-well Flexiperm chambers on perminox slides coated with
439 Poly-L-Ornithine (3 µg/mL; Sigma-Aldrich; P2533) and laminin in Dulbecco's Modified
440 Eagle Medium (DMEM; 10 µg/mL; Thermo Fisher Scientific; 23017015). The myoblasts
441 were plated at 100,000 cells per well in culture media (high-glucose DMEM, 20% fetal
442 bovine serum, 1× Glutamine, pen-strep, Fungizone) and incubated at 37°C and 5.0%
443 CO_2. Twenty-four hours post-plating, the media was replaced with fusion media (high-

444 glucose DMEM, 10% horse serum, 1× Glutamine, Pen strep, Fungizone). Myoblasts were
445 then incubated for 3 to 7 days following the addition of fusion media to generate
446 myotubes. RNA was extracted from myotubes before fusion, 3, and 7 days post-fusion
447 using an Aurum Total RNA mini kit (Bio-Rad), following manufacturer's instructions.

448 ***Co-immunoprecipitation***

449 *Plasmid Constructs:* For the GST pull-down experiments and co-immunoprecipitation
450 studies, the coding sequences of extracellular domain of AChR subunits (α [amino acids
451 21-230], β [aa 26-238], δ [aa 25-248], ε [aa 21-239], and γ [aa 23-240], the signal
452 sequences were removed) were cloned into pGEX-4T1 vector. The coding sequence of
453 Lynx1 (amino acids 21-92) with the signal sequence and the GPI anchoring signal
454 removed (Reference: PMID: 21252236) was cloned either into pGEX-4T1 vector (for GST
455 tag) or pET-28a (+) vector for 6-His tag. The set of plasmids encoding the full-length α, β,
456 δ, and ε subunits of AChRs was a kind gift from Dr. Lin Mei (Augusta University, USA).
457 The plasmid pLynx1-mCherry, as described in Nichols et al.[18], was obtained from Dr.
458 Henry A. Lester through Addgene.

459 *Protein purification:* Bacteria expressing the GST-tagged proteins were incubated in the
460 GST lysis buffer (50 mM NaH2PO4, 300 mM NaCl, 10 µg/ml leupeptin, 10 µg/ml aprotinin,
461 1 µl/ml Triton X-100, 10 µg/ml DNase I, and 15 units/µl Lysozyme). Similarly, bacteria
462 expressing the 6-His tagged proteins were incubated in the His lysis buffer (50 mM Tris-
463 Cl (pH8.0), 100 mM NaCl, 5 mM Imidazole, 10 µg/ml leupeptin, 10 µg/ml aprotinin, 1 µl/ml
464 Triton X-100, 10 µg/ml DNase I, and 15 units/µl Lysozyme). The supernatants containing
465 the GST-fusion or 6-His fusion proteins were incubated overnight with 20 µl of equilibrated
466 glutathione beads and His60 Ni resin, respectively. The beads containing GST-tagged

467 proteins were washed three times with the GST -wash buffer (4.3 mM Na2HPO4, 1.47
468 mM KH2PO4, 137 mM NaCl, and 2.7 mM KCl). Similarly, the beads containing 6-His-
469 tagged proteins were washed three times with His wash buffer (50 mM Tris-Cl (pH8.0),
470 100 mM NaCl, 20 mM Imidazole). The proteins were eluted with elution buffer (10 mM
471 glutathione 50 mM Tris pH=8,0 for GST tagged protein and 200 mM imidazole in 50 mM
472 NaCl, 50 mM Tris pH=8,0 for 6-His tagged protein).

473 *Immunoprecipitation:* HEK293 cells were co-transfected with pLynx1-mCherry and four
474 subunits of AChR (α, β, δ and ε); the cells were lysed 36 hr after transfection, and the
475 immunoprecipitation was performed as previously described[69]. Briefly, the lysates were
476 centrifuged, and supernatants were incubated with Dynabeads (Cat No: 10003D;
477 Invitrogen, CA) and coated with anti-AChR antibody (Cat No: 838301, Biolegend, CA).
478 Beads were then washed three times with lysis buffer, resuspended in 2x sample buffer
479 and boiled for 5 min. The samples were resolved by SDS-PAGE electrophoresis and
480 analyzed with anti-RFP antibody (Cat No: 600-401-379, Rockland, PA).

481 *Purification of nAChR extracellular domains and Lynx1*: The GST-tagged ectodomains of
482 AChR subunits and Lynx1 (GST tagged or 6-His tagged) were purified as previously
483 described[70]. BL21 bacteria were transformed with the respective constructs, grown in 200
484 ml cultures at 18°C until A600 between 0.4 and 0.6. The expression was induced by 0.5
485 mM isopropyl 1-thio-β-d-galactopyranoside (IPTG) for 4 h at 18 °C. Bacteria were
486 collected, incubated for 30 min at 4 °C in lyses buffer (50 mM NaH2PO4, 300 mM NaCl,
487 10 µg/ml leupeptin, 10 µg/ml aprotinin, 1 µl/ml Triton X-100, 10 µg/ml DNase I, and 15
488 units/µl Lysozyme), lysed by sonication for 1 min, and centrifuged at 13,8 g for 30 min.
489 The supernatants containing the GST-fusion proteins were incubated overnight with 20

490 μl of equilibrated glutathione beads. The beads were washed three times with washing
491 buffer (4.3 mM Na2HPO4, 1.47 mM KH2PO4, 137 mM NaCl, and 2.7 mM KCl) and the
492 proteins were eluted with elution buffer (10 mM glutathione 50 mM Tris pH=8,0). Purified
493 GST-tagged proteins were used to coat 10 μl of glutathione beads. These were washed
494 three times with washing buffer, followed by addition of homogenates of HEK293 cells
495 transfected with pLynx1-Cherry, and then overnight incubation. The beads were washed
496 with washing buffer and boiled with 2x sample buffer. The precipitated proteins were
497 resolved by SDS-PAGE electrophoresis and detected with anti-Cherry or anti-GST (Cat
498 No: G7781, Sigma, St. Louis, MO) antibodies.

499 To determine the direct interaction of GST-Lynx1 with the ectodomain of α subunit of
500 AChR (GST-tagged), the GST-AChR protein was incubated with Streptavidin – Dynabead
501 (Cat No: 11205D, Thermo Fisher Scientific, MA) coated with BTX-biotin (Cat No: B1196,
502 Thermo Fisher Scientific, MA) for one hour. Beads were then washed three times with
503 lysis buffer, and incubated with the purified GST-Lynx1 overnight. Beads were then
504 washed three times with lysis buffer, resuspended in 2x sample buffer and boiled for 5
505 min. The samples were resolved by SDS-PAGE electrophoresis and analyzed with anti-
506 GST antibody.

507 For analyzing Lynx1 specificity for AChR subunits, purified GST-tagged AChR subunits
508 were used to coat 20 μl of glutathione beads. These beads were washed three times with
509 washing buffer, followed by incubation with the purified 6-His-Lynx1 overnight. The beads
510 were washed with washing buffer and eluted with elution buffer (10 mM glutathione 50
511 mM Tris pH=8,0). The eluted proteins were mixed with 2x sample buffer and were

512 resolved by SDS-PAGE electrophoresis and detected with anti-His (Cat No: 66005-1-Ig
513 Proteintech, IL) or anti-GST (Cat No: G7781, Sigma, St. Louis, MO) antibodies.

514 ***Lynx1 antibody generation***

515 An antibody against Lynx1 was developed following the methods previously outlined[71].
516 In brief, a piggyback transposon vector pXL-CAG-Zeomycin-2A and a piggyback
517 transposase vector pCAG-mPBorf were obtained as a gift from Dr. Joshua Sanes. The
518 Lynx1 sequence was cloned into the transposon vector following the 2A peptide
519 sequence. L-cells were co-transfected with pXL-CAG-Zeomycin-2A-Lynx1 and pCAG-
520 mPBorf. A stable cell line of Lynx1-expressing L-cells was generated by selection with
521 Zeomycin and expression analysis confirmed the presence of Lynx1 mRNA. An antibody
522 against mouse Lynx1 was generated by immunizing 1 month-old Lynx1-knockout mice
523 with Lynx1-expressing L cells. Total serum was collected from immunized mice after six
524 weeks of immunizations and purified using acetone powder. Antibody specificity was
525 verified using transfected L cells and knockout mouse tissue.

526 ***Electrophysiology recordings:***

527 *Nerve-muscle preparations:* Nerve–muscle preparations of the Extensor digitorum longus
528 muscle (EDL) were dissected in oxygenated physiological solution (in mM): 110 NaCl, 5
529 KCl, 1 MgCl2, 25 NaHCO3, 2 CaCl2, 11 glucose, 0.3 glutamic acid, 0.4 glutamine, 5 BES
530 (N,N-Bis(2-hydroxyethyl)-2-aminoethanesulfonic acid sodium salt), 0.036 choline
531 chloride, and 4.34x10-7 cocarboxylase. After dissection, nerve muscle preparations were
532 pinned in a Sylgard-coated recording chamber constantly perfused with oxygenated
533 physiological solution (95%O2, 5%CO2). The pH (7.4) and temperature (28 ±2°C) were
534 continuously regulated.

535 *Recordings of synaptic transmission:* Only recordings with an initial membrane potential
536 larger than -65 mV and with less than 5 mV variation from holding potential were included
537 in the analysis. NMJs were located using bright field illumination of an upright Olympus
538 microscope with a 60X objective. Muscle fibers were impaled 50-100 μm from the NMJ
539 to be studied, avoiding mechanical distortion of the NMJ.

540 Stimulation of the deep peroneal nerve was performed using a suction electrode filled
541 with extracellular saline. Endplate potentials (EPPs) were recorded using glass
542 microelectrodes (1.0 mm OD; WPI) pulled to 40-70 MΩ (filled with 3mM KCl) with a P-70
543 Brown-Flaming micropipette puller (Sutter Instruments). Synaptic responses were
544 amplified by an AM Systems 1600 amplifier and further amplified (100x) and filtered (2
545 kHz) by a Warner Instruments DC amplifier. The recordings were digitized (10 KHz) using
546 a National Instruments BNC 2110 board and subsequently acquired with WinWCP
547 software (John Dempster, Strathclyde University, Strathclyde, UK).

548 Synaptic strength was determined by measuring the paired pulse facilitation (PPF) and
549 the quantal content (m). These were obtained using a low Ca^{2+} (1mM) and high Mg^{2+}
550 (7.0mM) modified physiological solution. Miniature endplate potentials (MEPPs)
551 amplitude and frequency were first determined during a 5-10 min period of recordings
552 without motor nerve stimulation. PPF was then obtained using two stimuli (0.1 ms
553 duration, 10 ms interval), elicited at 0.2 Hz. Quantal content (m) was determined using
554 the amplitude of the first EPP (EPP1) and MEPPs (mean EPP1s amp/mean MEPPs
555 amp). Four to seven NMJs were studied per muscle.

556 Following a baseline recording of 20 min (0.2 Hz), synaptic plasticity was elicited by a
557 sustained motor nerve stimulation (120 Hz, 10 s) followed by 45 min recordings of EPPs

558 evoked at 0.2 Hz. Muscle contractions were prevented with partial blockade of the
559 postsynaptic ACh receptors using D-tubocurarine (2.0 μM. Sigma). Only one NMJ was
560 studied per muscle.

561 *Muscular and neuromuscular strength and fatigue:* EDL nerve-muscle preparations were
562 attached to a fixed force transducer (model 402A-500mN, Aurora Scientific Inc) at one
563 end and an adjustable hook at the other end, using surgical thread. The knots for
564 attaching the muscle to the force transducer and the hook were done at the level of the
565 tendons, under a binocular, to prevent muscle fiber damage. Muscles were maintained
566 vertically in a 140 ml beaker containing oxygenated physiological solution. Two sets of
567 stimulating electrodes were then put in place. First, two platinum wires were positioned
568 on the muscle and on the tendon to stimulate the muscle directly. Second, the cut end of
569 the deep peroneal nerve was stabilized in a stimulating suction electrode filled with
570 extracellular saline. Nerve and muscle stimulations were performed either alternatively or
571 simultaneously.

572 Muscular and neuro-muscular twitch force responses were elicited by means of single
573 supra-maximal square-wave pulses lasting 1 ms and 0.1 ms, respectively. Optimal
574 muscle length was determined by incrementally stretching the muscle until maximum
575 neuro-muscular twitch force output was attained. After each length adjustment, a two-
576 minute rest period was allowed before the next stimulation.

577 The fatigue protocol consisted of bouts of motor nerve stimulations (120Hz, 300 ms) at
578 1Hz, for 3 min. Muscular stimulations were super-imposed on nerve stimulations at the
579 2nd, 10th, 20th, 30th stimulation, and so on until the end of the fatigue protocol so that both
580 muscular and neuromuscular fatigue could be measured. This was followed by a 30 min

581 recovery period where muscular and neuromuscular strength were measured at 2s, 5s,
582 10s, 15s, 30s, 1min, 1.5 min, 2 min, 2.5 m in, 5 min, 10 min, 20 min and 30 min following
583 the fatigue protocol.

584 ***Immunohistochemistry and confocal microscopy of EDL muscles***

585 EDL muscles from mice expressing YFP in nerve endings were used to visualize NMJs.
586 Following perfusion, muscles were dissected and incubated with alexa-555 bungarotoxin
587 (Life Technologies, 1:1000 in 1XPBS) for 1 hour. Muscles were then washed 3 times with
588 1XPBS and whole mounted using vectashield. NMJs were imaged using a Zeiss LSM
589 700 confocal microscope. Maximum intensity projections from confocal z-stacks were
590 created using Zen Black (Zeiss) and analyzed using ImageJ.

591 *NMJ Analysis:* Structural features were analyzed based on previously described methods
592 in Valdez et al. 2010[65]. In brief, full or partial denervation of NMJs is classified by
593 inadequate apposition of YFP and BTX while fragmented nAChRs are defined as having
594 5 or more islands in the cluster. Sprouting NMJs are those with a nerve terminal
595 overreaching the nAChR cluster. NMJs with multiple innervation are those with more than
596 one axon innervating a single nAChR cluster. The endplate area is a measurement of the
597 total area occupied by nAChR clusters in a single muscle. Colocalization is a
598 measurement of YFP and BTX apposition analyzed using the ImageJ colocalization
599 plugin. nAChR intensity was determined from the mean integrated density of nAChR
600 clusters using ImageJ.

601 ***Immunohistochemistry and confocal microscopy of TA sections***

602 Following perfusion, TA muscles were dissected and incubated in 30% sucrose for 48
603 hours at 4°C. Muscles were then cut in half and placed in Fisherbrand base molds with

604 Tissue Freezing Medium (Triangle Biomedical Sciences, Inc.) Using a cryostat, TA
605 muscles were sectioned at 16 μm thickness and collected on gelatin-coated slides.
606 Sections were first washed 3 times with 1XPBS and then incubated for 1 hour at room
607 temperature with wheat germ agglutinin conjugated with alexa-555 (WGA, 1:700) and
608 DAPI (4'6-diamidino-2-phenylindole: Sigma-Aldrich; 28718-90-3; 1:1,000) diluted in
609 1XPBS. Muscles were then washed 3 times with 1XPBS and whole mounted using
610 vectashield. Muscle fibers were imaged using a Zeiss LSM 700 confocal microscope.
611 Maximum intensity projections from confocal z-stacks were created using Zen Black
612 (Zeiss) and analyzed using ImageJ. Muscle fibers were outlined by WGA and measured
613 in ImageJ using the grid to randomly select at least 100 fibers per mouse to analyze fiber
614 area. The percentage of centralized nuclei was then determined using the localization of
615 DAPI in the outlined muscle fibers.

616 ***Immunohistochemistry and confocal microscopy for fiber-typing***

617 TA muscles were immediately dissected following aesthesia with isoflurane and flash
618 frozen in liquid nitrogen. Muscles were then cut in half and placed in Fisherbrand base
619 molds with Tissue Freezing Medium (Triangle Biomedical Sciences, Inc.). Using a
620 cryostat, TA muscles were sectioned at 16 μm thickness and collected on gelatin-coated
621 slides. Sections were first washed 3 times with 1XPBS and then incubated for 1 hour at
622 room temperature in blocking buffer (0.1% Triton X-100, 3% BSA, and 5% goat serum in
623 1XPBS). Next, sections were incubated with primary antibodies diluted in 3% BSA and
624 5% goat serum in 1XPBS overnight at 4°C. The following primary antibodies were used:
625 rabbit-anti-laminin (1:300), IgG2b-BAD5 (1:20) to label MyHCI, IgM-BF-F3 (1:20) to label
626 MyHCIIb, and IgG1-SC71 (1:40) to label MyHCIIa. Sections were then washed 3 times

627 with 1XPBS and incubated for 2 hours at room temperature with secondary antibodies
628 and 4',6-diamidino-2-phenylindole (DAPI, Sigma, 1:1000). The following secondary
629 antibodies were used: alexa-568 anti-mouse IgM (Life Technologies, 1:1000), alexa-488
630 donkey anti-rabbit (Life Technologies, 1:1000), and alexa-647 anti-mouse IgG1 (Life
631 Technologies, 1:1000). Slides were then washed 3 times with 1XPBS and mounted using
632 vectashield. Muscle sections were imaged using a Zeiss LSM 700 motorized confocal
633 microscope. Maximum intensity projections from confocal z-stacks were created using
634 Zen Black (Zeiss). The percentages of MyHCIIa and MyHCIIb fibers were determined
635 based on the number of SC-71 and BF-F3 positive fibers, respectively.

636 ***qPCR expression analysis***

637 Mice were anesthetized with isoflurane, and TA muscles were immediately dissected and
638 flash frozen in liquid nitrogen. RNA was prepared using an Aurum Total RNA Mini kit (Bio-
639 Rad), following the manufacturer's instructions. cDNA was then synthesized from 100ng
640 of total RNA using an iScript cDNA synthesis kit (Bio-Rad). PCR amplification was
641 performed on the Bio-Rad CFX Connect Real-Time System (Bio-Rad) using iTaq
642 Universal SYBR Green Supermix (Bio-Rad). The primers used in this study are listed in
643 Supplementary Table 1.

644 ***nAChR turnover analysis***

645 The labeling of distinct nAChR pools was performed as described in Bruneau et al.,[47] with
646 slight modification. Male C57/BL6 and Lynx1$^{-/-}$ mice, aged 148 days, were anesthetized
647 by an intraperitoneal injection (5μL/g) of a mixed solution of ketamine (100mg/mL) and
648 xylazine (20mg/mL) in sterile 0.9% saline. Each mouse was placed on its back and the
649 sternomastoid muscle was surgically exposed. Muscles were bathed in saturating levels

650 of alexa 488-conjugated α-bungarotoxin (5μg/mL) for 1.5 h and then washed with sterile
651 saline 3 times for 5 minutes. Two days following exposure, the animals were perfused
652 transcardially with 4% PFA and the sternomastoid muscles were dissected. Muscles were
653 then incubated with alexa 555-conjugated α-bungarotoxin (5μg/mL) for 1.5 h and then
654 washed with sterile saline 3 times for 5 minutes each. Whole Sternomastoid muscles were
655 mounted using vectashield and imaged with a Zeiss LSM 710 confocal microscope with
656 the same scanning parameters. Maximum intensity projections from confocal z-stacks
657 were created using Zen Black (Zeiss). The intensity of the 488 and 555 channels were
658 analyzed at individual NMJs using ImageJ. The ratio of 555 to overall intensity was
659 calculated for each NMJ and averaged for each animal. This ratio is considered the
660 percentage of new nAChRs present.

661 ***Spinal Cord analysis***

662 Spinal columns were dissected immediately after perfusion and post-fixed in 4%
663 paraformaldehyde (PFA) overnight at 4°C. Following post-fixation, the spinal column was
664 washed three times with 1xPBS and then cut in half at the last rib to separate the lumbar
665 and sacral regions from the thoracic and cervical regions. The different regions of the
666 spinal cord were isolated and placed in 30% sucrose overnight at 4°C. The spinal cord
667 segments were then placed in a Fisherbrand base mold with Tissue Freezing Medium
668 from Triangle Biomedical Sciences, Inc. Using a cryostat, 30 μm sections were collected
669 on gelatin-coated slides and subsequently mounted using Vectashield. Ventral horns
670 were imaged with a Zeiss LSM 900 confocal microscope with the same scanning
671 parameters. Maximum intensity projections from confocal z-stacks were created using

672 Zen Black (Zeiss). The area of each motor neuron in the ventral horn was measured using
673 ImageJ.

674 ***Statistics***

675 For comparisons between two experimental groups, unpaired two-sided Student's t-tests
676 were used to determine significance. For comparisons between two sample distributions,
677 Kolmogorov–Smirnov tests were used to determine significance. Bar graphs are
678 represented as means ± standard error. Data values and p-values are reported within the
679 text. All measurements were taken from distinct samples with the sample size (*n*) listed
680 in the figure legends. Statistical analysis was performed using R statistics software and
681 GraphPad Prism7 with a p-value <0.05 was considered significant.

682

683 **References**

684 1. Sarter M, Bruno JP, Parikh V. Abnormal Neurotransmitter Release Underlying
685 Behavioral and Cognitive Disorders: Toward Concepts of Dynamic and Function-
686 Specific Dysregulation. *Neuropsychopharmacology*. 2007;32(7):1452-1461.
687 doi:10.1038/sj.npp.1301285

688 2. Millar NS, Harkness PC. Assembly and trafficking of nicotinic acetylcholine
689 receptors (Review). *Mol Membr Biol*. 2008;25(4):279-292.
690 doi:10.1080/09687680802035675

691 3. Missias AC, Chu GC, Klocke BJ, Sanes JR, Merlie JP. Maturation of the
692 acetylcholine receptor in skeletal muscle: regulation of the AChR gamma-to-epsilon
693 switch. *Dev Biol*. 1996;179(1):223-238. doi:10.1006/dbio.1996.0253

694 4. Schaeffer L, De Kerchove D'Exaerde A, Changeux JP. Targeting transcription to
695 the neuromuscular synapse. *Neuron*. 2001;31(1):15-22. doi:10.1016/S0896-
696 6273(01)00353-1

697 5. Yumoto N, Wakatsuki S, Sehara-Fujisawa A. The acetylcholine receptor γ-to-ε
698 switch occurs in individual endplates. *Biochem Biophys Res Commun*.
699 2005;331(4):1522-1527. doi:10.1016/j.bbrc.2005.04.081

700 6. Witzemann V, Schwarz H, Koenen M, et al. Acetylcholine receptor ε-subunit
701 deletion causes muscle weakness and atrophy in juvenile and adult mice. *Proc Natl*
702 *Acad Sci U S A*. 1996;93(23):13286-13291. doi:10.1073/pnas.93.23.13286

703 7. Middleton L, Ohno K, Christodoulou K, et al. Chromosome 17p-linked myasthenias
704 stem from defects in the acetylcholine receptor epsilon-subunit gene. *Neurology*.
705 1999;53(5):1076-1082. doi:10.1212/wnl.53.5.1076

706 8. Ohno K, Anlar B, Özdirim E, Brengman JM, Engel AG. Frameshifting and splice-
707 site mutations in the acetylcholine receptor ε subunit gene in three Turkish kinships
708 with congenital myasthenic syndromes. In: *Annals of the New York Academy of*
709 *Sciences*. Vol 841. Blackwell Publishing Inc.; 1998:189-194. doi:10.1111/j.1749-
710 6632.1998.tb10926.x

711 9. Ohno K, Anlar B, Özdirim E, Brengman JM, DeBleecker JL, Engel AG. Myasthenic
712 syndromes in Turkish kinships due to mutations in the acetylcholine receptor. *Ann*
713 *Neurol*. 1998;44(2):234-241. doi:10.1002/ana.410440214

714 10. Ohno K, Quiram PA, Milone M, et al. Congenital myasthenic syndromes due to
715 heteroallelic nonsense/missense mutations in the acetylcholine receptor ε subunit

716 gene: Identification and functional characterization of six new mutations. *Hum Mol*
717 *Genet*. 1997;6(5):753-766. doi:10.1093/hmg/6.5.753

718 11. Engel AG, Ohno K, Bouzat C, Sine SM, Griggs RC. End-plate acetylcholine
719 receptor deficiency due to nonsense mutations in the ε subunit. *Ann Neurol*.
720 1996;40(5):810-817. doi:10.1002/ana.410400521

721 12. Croxen R, Young C, Slater C, et al. End-plate gamma- and epsilon-subunit mRNA
722 levels in AChR deficiency syndrome due to epsilon-subunit null mutations. *Brain*.
723 2001;124(Pt 7):1362-1372. doi:10.1093/brain/124.7.1362

724 13. Misgeld T, Kummer TT, Lichtman JW, Sanes JR. Agrin promotes synaptic
725 differentiation by counteracting an inhibitory effect of neurotransmitter. *Proc Natl*
726 *Acad Sci U S A*. 2005;102(31):11088-11093. doi:10.1073/pnas.0504806102

727 14. Misgeld T, Burgess RW, Lewis RM, Cunningham JM, Lichtman JW, Sanes JR.
728 Roles of neurotransmitter in synapse formation: development of neuromuscular
729 junctions lacking choline acetyltransferase. *Neuron*. 2002;36(4):635-648.
730 http://www.ncbi.nlm.nih.gov/pubmed/12441053. Accessed February 12, 2016.

731 15. Lanuza MA, Besalduch N, González C, et al. Decreased phosphorylation of delta
732 and epsilon subunits of the acetylcholine receptor coincides with delayed
733 postsynaptic maturation in PKC theta deficient mouse. *Exp Neurol*.
734 2010;225(1):183-195. doi:10.1016/J.EXPNEUROL.2010.06.014

735 16. Leenders AGM, Sheng Z-H. Modulation of neurotransmitter release by the second
736 messenger-activated protein kinases: implications for presynaptic plasticity.
737 *Pharmacol Ther*. 2005;105(1):69-84. doi:10.1016/j.pharmthera.2004.10.012

738 17. Smith DO, Williams KD, Emmerling M. Changes in acetylcholine receptor
739 distribution and binding properties at the neuromuscular junction during aging. *Int*
740 *J Dev Neurosci*. 1990;8(6):629-642.

741 18. Friese MB, Blagden CS, Burden SJ. Synaptic differentiation is defective in mice
742 lacking acetylcholine receptor β-subunit tyrosine phosphorylation. *Development*.
743 2007;134(23):4167-4176. doi:10.1242/dev.010702

744 19. Sugita S, Fleming LL, Wood C, et al. VAChT overexpression increases
745 acetylcholine at the synaptic cleft and accelerates aging of neuromuscular
746 junctions. *Skelet Muscle*. 2016;6(1). doi:10.1186/s13395-016-0105-7

747 20. Magalhães-Gomes MPS, Motta-Santos D, Schetino LPL, et al. Fast and slow-
748 twitching muscles are differentially affected by reduced cholinergic transmission in
749 mice deficient for VAChT: A mouse model for congenital myasthenia. *Neurochem*
750 *Int*. 2018;120. doi:10.1016/j.neuint.2018.07.002

751 21. Vaughan SK, Sutherland NM, Valdez G. Attenuating Cholinergic Transmission
752 Increases the Number of Satellite Cells and Preserves Muscle Mass in Old Age.
753 *Front Aging Neurosci*. 2019;11:262. doi:10.3389/fnagi.2019.00262

754 22. Palma E, Reyes-Ruiz JM, Lopergolo D, et al. Acetylcholine receptors from human
755 muscle as pharmacological targets for ALS therapy. *Proc Natl Acad Sci U S A*.
756 2016;113(11):3060-3065. doi:10.1073/pnas.1600251113

757 23. Melroy-Greif WE, Stitzel JA, Ehringer MA. Nicotinic acetylcholine receptors:
758 upregulation, age-related effects and associations with drug use. *Genes Brain*
759 *Behav*. 2016;15(1):89-107. doi:10.1111/gbb.12251

760 24. Arbour D, Tremblay E, Martineau E, Julien J-P, Robitaille R. Early and Persistent
761 Abnormal Decoding by Glial Cells at the Neuromuscular Junction in an ALS Model.
762 *J Neurosci*. 2015;35(2):688-706. doi:10.1523/JNEUROSCI.1379-14.2015

763 25. Rocha MC, Pousinha PA, Correia AM, Sebastião AM, Ribeiro JA. Early changes of
764 neuromuscular transmission in the SOD1(G93A) mice model of ALS start long
765 before motor symptoms onset. *PLoS One*. 2013;8(9):e73846.
766 doi:10.1371/journal.pone.0073846

767 26. Pousinha PA, Correia AM, Sebastião AM, Ribeiro JA. The giant miniature endplate
768 potentials frequency is increased in aged rats. *Neurosci Lett*. 2015;584:224-229.
769 doi:10.1016/j.neulet.2014.10.035

770 27. Sugita S, Fleming LL, Wood C, et al. VAChT overexpression increases
771 acetylcholine at the synaptic cleft and accelerates aging of neuromuscular
772 junctions. *Skelet Muscle*. 2016;6(1):31. doi:10.1186/s13395-016-0105-7

773 28. Miwa JM, Miwa JM, Ibanez-Tallon I, et al. lynx 1, an Endogenous Toxin-like
774 Modulator of Nicotinic Acetylcholine Receptors in the mammalian CNS. *Neuron*.
775 1999;23:0.

776 29. Parker RL, O'Neill HC, Henley BM, et al. Deletion of lynx1 reduces the function of
777 α6* nicotinic receptors. Akaaboune M, ed. *PLoS One*. 2017;12(12):e0188715.
778 doi:10.1371/journal.pone.0188715

779 30. George AA, Bloy A, Miwa JM, Lindstrom JM, Lukas RJ, Whiteaker P. Isoform-
780 specific mechanisms of α3β4*-nicotinic acetylcholine receptor modulation by the
781 prototoxin lynx1. *FASEB J*. 2017;31(4):1398-1420. doi:10.1096/fj.201600733R

782 31. Ibanez-Tallon I, Miwa JM, Wang HL, et al. Novel modulation of neuronal nicotinic
783 acetylcholine receptors by association with endogenous prototoxin lyn1. *Neuron*.
784 2002;33(6):893-903.

785 32. Nichols WA, Henderson BJ, Yu C, et al. Lynx1 Shifts 4 2 Nicotinic Receptor
786 Subunit Stoichiometry by Affecting Assembly in the Endoplasmic Reticulum. *J Biol*
787 *Chem*. 2014;289(45):31423-31432. doi:10.1074/jbc.M114.573667

788 33. Sajo M, Ellis-Davies G, Morishita H. Lynx1 Limits Dendritic Spine Turnover in the
789 Adult Visual Cortex. *J Neurosci*. 2016;36(36):9472-9478.
790 doi:10.1523/JNEUROSCI.0580-16.2016

791 34. Morishita H, Miwa JM, Heintz N, Hensch TK. Lynx1, a cholinergic brake, limits
792 plasticity in adult visual cortex. *Science*. 2010;330(6008):1238-1240.
793 doi:10.1126/science.1195320

794 35. Takesian AE, Bogart LJ, Lichtman JW, Hensch TK. Inhibitory circuit gating of
795 auditory critical-period plasticity. *Nat Neurosci*. 2018;21(2):218-227.
796 doi:10.1038/s41593-017-0064-2

797 36. Kobayashi A, Parker RL, Wright AP, et al. lynx1 Supports Neuronal Health in the
798 Mouse Dorsal Striatum During Aging: an Ultrastructural Investigation. *J Mol*
799 *Neurosci*. 2014;53(3):525-536. doi:10.1007/s12031-014-0352-1

800 37. Miwa JM, Walz A. Enhancement in Motor Learning through Genetic Manipulation
801 of the Lynx1 Gene. *PLoS One*. 2012;7(11). doi:10.1371/

802 38. Sanz E, Yang L, Su T, Morris DR, McKnight GS, Amieux PS. Cell-type-specific

803 isolation of ribosome-associated mRNA from complex tissues. *Proc Natl Acad Sci*
804 *U S A*. 2009;106(33):13939-13944. doi:10.1073/pnas.0907143106

805 39. Hippenmeyer S, Vrieseling E, Sigrist M, et al. A developmental switch in the
806 response of DRG neurons to ETS transcription factor signaling. *PLoS Biol*.
807 2005;3(5):e159. doi:10.1371/journal.pbio.0030159

808 40. Miwa JM, Stevens TR, King SL, et al. The Prototoxin lynx1 Acts on Nicotinic
809 Acetylcholine Receptors to Balance Neuronal Activity and Survival In Vivo. *Neuron*.
810 2006;51(5):587-600. doi:10.1016/j.neuron.2006.07.025

811 41. Lyukmanova EN, Shulepko MA, Buldakova SL, et al. Water-soluble LYNX1
812 Residues Important for Interaction with Muscle-type and/or Neuronal Nicotinic
813 Receptors. *J Biol Chem*. 2013;288(22):15888-15899.
814 doi:10.1074/jbc.M112.436576

815 42. Sanes JR, Lichtman JW. Development of the Vertebrate Neuromuscular Junction.
816 *Annu Rev Neurosci*. 1999;22(1):389-442. doi:10.1146/annurev.neuro.22.1.389

817 43. Zammit PS, Relaix F, Nagata Y, et al. Pax7 and myogenic progression in skeletal
818 muscle satellite cells. *J Cell Sci*. 2006;119(9):1824-1832. doi:10.1242/jcs.02908

819 44. Venuti JM, Morris JH, Vivian JL, Olson EN, Klein WH. Myogenin is required for late
820 but not early aspects of myogenesis during mouse development. *J Cell Biol*.
821 1995;128(4):563-576. doi:10.1083/jcb.128.4.563

822 45. Burden SJ, Yumoto N, Zhang W. The role of MuSK in synapse formation and
823 neuromuscular disease. *Cold Spring Harb Perspect Biol*. 2013;5(5).

824 doi:10.1101/cshperspect.a009167

825 46. Lee Y, Rudell J, Ferns M. Rapsyn interacts with the muscle acetylcholine receptor
826 via α-helical domains in the α, β, and ε subunit intracellular loops. *Neuroscience*.
827 2009;163(1):222-232. doi:10.1016/j.neuroscience.2009.05.057

828 47. Bruneau E, Sutter D, Hume RI, Akaaboune M. Identification of Nicotinic
829 Acetylcholine Receptor Recycling and Its Role in Maintaining Receptor Density at
830 the Neuromuscular Junction In Vivo. 2005. doi:10.1523/JNEUROSCI.3169-
831 05.2005

832 48. Evans WJ, Lexell J. Human Aging, Muscle Mass, and Fiber Type Composition.
833 *Journals Gerontol Ser A Biol Sci Med Sci*. 1995;50A(Special):11-16.
834 doi:10.1093/gerona/50A.Special_Issue.11

835 49. Frontera WR, Miljkovic N, Lim J-Y, Miljkovic I. Aging of Skeletal Muscle Fibers. *Ann*
836 *Rehabil Med Rev Artic Ann Rehabil Med*. 2015;39(2):155-162.
837 doi:10.5535/arm.2015.39.2.155

838 50. Frontera WR, Reid KF, Phillips EM, et al. Muscle fiber size and function in elderly
839 humans: a longitudinal study. *J Appl Physiol*. 2008;105(2):637-642.
840 doi:10.1152/japplphysiol.90332.2008

841 51. Meyer MA. Identification of 17 highly expressed genes within mouse lumbar spinal
842 cord anterior horn region from an in-situ hybridization atlas of 3430 genes:
843 implications for motor neuron disease. *Neurol Int*. 2014;6(2):5367.
844 doi:10.4081/ni.2014.5367

845 52. Nabel EM, Morishita H. Regulating Critical Period Plasticity: Insight from the Visual
846 System to Fear Circuitry for Therapeutic Interventions. *Front Psychiatry*.
847 2013;4:146. doi:10.3389/fpsyt.2013.00146

848 53. Thomsen MS, Arvaniti M, Jensen MM, et al. Lynx1 and Aβ1-42 bind competitively
849 to multiple nicotinic acetylcholine receptor subtypes. 2016.
850 doi:10.1016/j.neurobiolaging.2016.06.009

851 54. Nissen NI, Anderson KR, Wang H, et al. Augmenting the antinociceptive effects of
852 nicotinic acetylcholine receptor activity through lynx1 modulation. *PLoS One*.
853 2018;13(7). doi:10.1371/journal.pone.0199643

854 55. Hall ZW. Alpha neurotoxins and their relatives: foes and friends? *Neuron*.
855 1999;23(1):4-5.

856 56. Shulepko MA, Lyukmanova EN, Kasheverov IE, Dolgikh DA, Tsetlin VI,
857 Kirpichnikov MP. Bacterial expression of the water-soluble domain of lynx1, an
858 endogenous neuromodulator of human nicotinic receptors. *Russ J Bioorganic*
859 *Chem*. 2011;37(5):543-549. doi:10.1134/S1068162011050165

860 57. Banker BQ, Kelly SS, Robbins N. Neuromuscular transmission and correlative
861 morphology in young and old mice. *J Physiol*. 1983;339:355-377.

862 58. Kelly SS. The effect of age on neuromuscular transmission. *J Physiol*.
863 1978;274(1):51-62. doi:10.1113/jphysiol.1978.sp012133

864 59. Tremblay E, Martineau É, Robitaille R. Opposite Synaptic Alterations at the
865 Neuromuscular Junction in an ALS Mouse Model: When Motor Units Matter. *J*

866 *Neurosci*. 2017;37(37):8901-8918. doi:10.1523/JNEUROSCI.3090-16.2017

867 60. Willadt S, Nash M, Slater C. Age-related changes in the structure and function of
868 mammalian neuromuscular junctions. *Ann N Y Acad Sci*. 2018;1412(1):41-53.
869 doi:10.1111/nyas.13521

870 61. Courtney J, Steinbach JH. Age changes in neuromuscular junction morphology and
871 acetylcholine receptor distribution on rat skeletal muscle fibres. *J Physiol*.
872 1981;320:435-447. doi:10.1113/jphysiol.1981.sp013960

873 62. Cheng A, Morsch M, Murata Y, Ghazanfari N, Reddel SW, Phillips WD. Sequence
874 of Age-Associated Changes to the Mouse Neuromuscular Junction and the
875 Protective Effects of Voluntary Exercise. *PLoS One*. 2013.
876 doi:10.1371/journal.pone.0067970

877 63. Li Y, Lee Y i., Thompson WJ. Changes in Aging Mouse Neuromuscular Junctions
878 Are Explained by Degeneration and Regeneration of Muscle Fiber Segments at the
879 Synapse. *J Neurosci*. 2011. doi:10.1523/jneurosci.3590-11.2011

880 64. Valdez G, Heyer MP, Feng G, Sanes JR. The role of muscle microRNAs in repairing
881 the neuromuscular junction. *PLoS One*. 2014;9(3):e93140.
882 doi:10.1371/journal.pone.0093140

883 65. Valdez G, Tapia JC, Kang H, et al. Attenuation of age-related changes in mouse
884 neuromuscular synapses by caloric restriction and exercise. *Proc Natl Acad Sci U*
885 *S A*. 2010;107(33):14863-14868. doi:1002220107 [pii]10.1073/pnas.1002220107

886 66. Dalkin W, Taetzsch T, Valdez G. The Fibular Nerve Injury Method: A Reliable Assay

887 to Identify and Test Factors That Repair Neuromuscular Junctions. *J Vis Exp*.
888 2016;(114). doi:10.3791/54186

889 67. Deschenes MR, Kressin KA, Garratt RN, Leathrum CM, Shaffrey EC. Effects of
890 exercise training on neuromuscular junction morphology and pre- to post-synaptic
891 coupling in young and aged rats. *Neuroscience*. 2016;316:167-177.
892 doi:10.1016/j.neuroscience.2015.12.004

893 68. Feng G, Mellor RH, Bernstein M, et al. Imaging Neuronal Subsets in Transgenic
894 Mice Expressing Multiple Spectral Variants of GFP. *Neuron*. 2000;28(1):41-51.
895 doi:10.1016/S0896-6273(00)00084-2

896 69. Gingras J, Gawor M, Bernadzki KM, et al. α-Dystrobrevin-1 recruits Grb2 and α-
897 catulin to organize neurotransmitter receptors at the neuromuscular junction. *J Cell*
898 *Sci*. 2016. doi:10.1242/jcs.181180

899 70. Herrmann D, Straubinger M, Hashemolhosseini S. Protein kinase CK2 interacts at
900 the neuromuscular synapse with Rapsyn, Rac1, 14-3-3γ, and Dok-7 proteins and
901 phosphorylates the latter two. *J Biol Chem*. 2015. doi:10.1074/jbc.M115.647610

902 71. Goodman KM, Yamagata M, Jin X, et al. Molecular basis of sidekick-mediated cell-
903 cell adhesion and specificity. *Elife*. 2016;5:e19058. doi:10.7554/eLife.19058

904 **Acknowledgements**

905 This work was funded through grants from the National Institute on Aging (R01AG055545
906 and R56AG051501) and the National Institute of Neurological Disorders and Stroke
907 (R21NS106313) awarded to GV. A portion of this work was also funded from a grant from
908 National Science Center, Poland (UMO-2018/29/B/NZ3/02675) awarded to TJP, and by a

grant from Canadian Institute for Health Research (MOP-111070) and a discovery grant from the Natural Science and Engineering Research Council to RR. SBA was a Banting research scholar from Canadian Institute for Health Research.

Author Contributions

Study concept and design: SKV, GV. Acquisition of data: SKV and GV contributed to all aspects of the manuscript, SBA and RR contributed to electrophysiological studies, TJP and BPS contributed to co-immunoprecipitation experiments, TM contributed to data analysis. Drafting the manuscript: SKV, SBA, GV, RR. Statistical analysis: SKV, SB, TM, GV. Obtained funding: GV, RR, and TJP.

Conflicts of Interest

The authors have no conflict of interest to declare.

Data Availability

Data generated from the experiments outlined in this manuscript are available upon request from the corresponding author.

Figures

Figure 1.

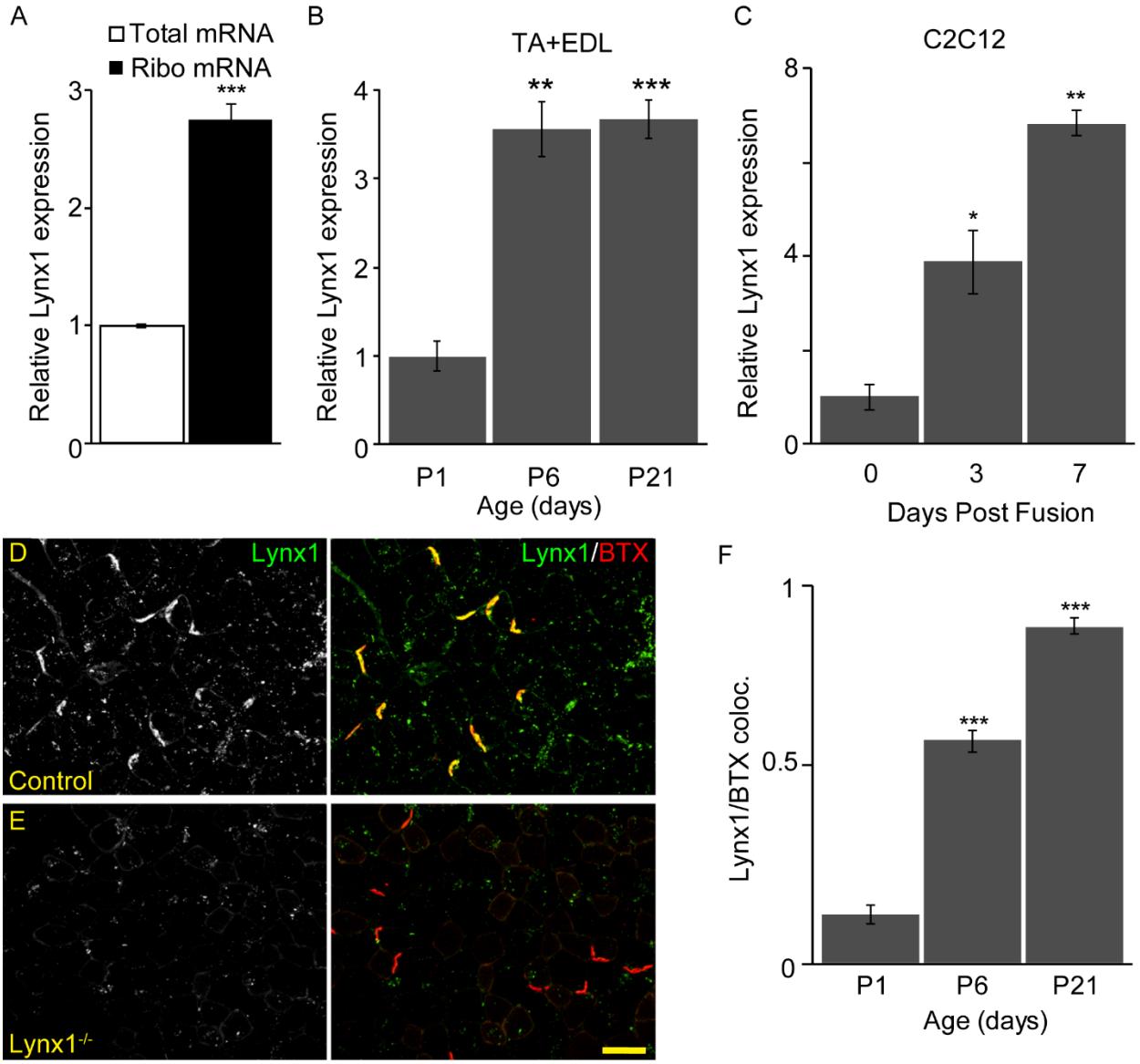

Figure 1. Skeletal muscles express Lynx1 at the NMJ. Lynx1 mRNA is enriched in ribosomal mRNA fractions obtained from adult TA muscle compared to total muscle mRNA (A). Lynx1 mRNA expression is detected in TA and EDL muscles and is significantly upregulated at postnatal day 6 (P6) and 21 (P21), relative to postnatal day 1 (P1) (B). Lynx1 mRNA is expressed in C2C12 myotubes and is significantly upregulated at 3 and 7 days post-fusion compared to unfused myoblasts (C). Lynx1 protein is colocalized with BTX in control TA muscles (D), but colocalization is not present in Lynx1$^{-/-}$ muscles (E). In control muscles, Lynx1 colocalization with BTX is significantly increased at P6 and P21, relative to P1 (F). Data represented as means ± SEM. Expression is normalized to GAPDH and relative to control. All male mice were used for this study. IP n=4; P1, P6, P21 n=5; C2C12 experiments were conducted with at least three biological replicates. D-E are representative images of P21 TA muscles. At least 30 NMJs were analyzed per animal (H). Scale bar=20 µm. Statistical significance was determined with unpaired and two-sided Student's t-tests. *p<0.05, **p<0.01, ***p<0.001.

Figure 2.

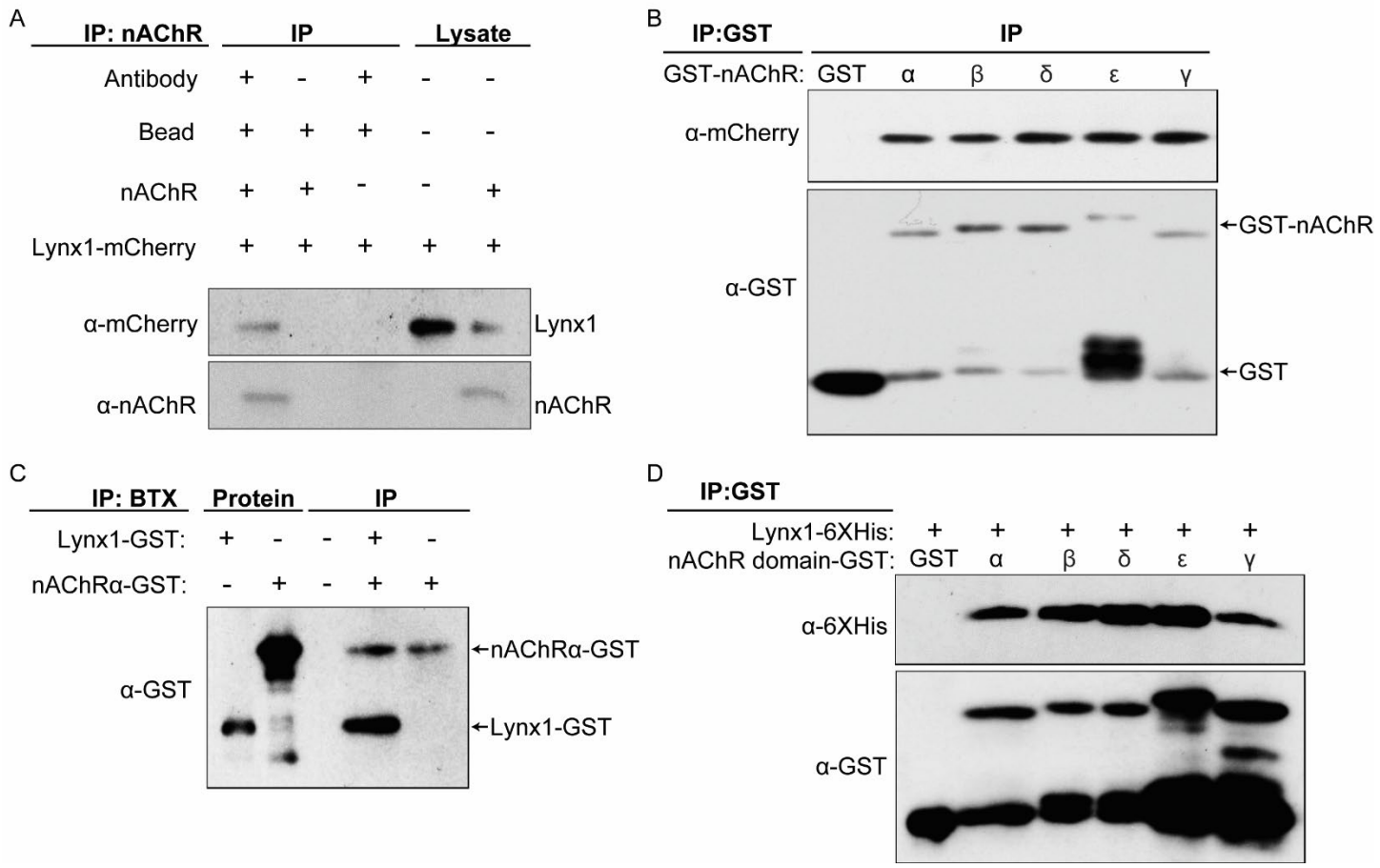

Figure 2. Lynx1 interacts with nAChRs. HEK293 cells were co-transfected with pLynx1-mCherry and four subunits of nAChR (α, β, δ and ε) that make functional receptors. The pull-down was performed with anti-nAChR antibody, and the blot was probed with anti-RFP or anti-nAChR antibodies. pLynx1-mCherry co-precipitates with nAChRs from HEK293 cell extract (A). The middle lane in the IP represents a control for precipitation specificity (beads without anti-nAChR antibody). The extracellular domains of each nAChR subunit (α, β, δ, ε and γ) were purified from bacteria and were analyzed for their ability pull-down Lynx1-Cherry from the HEK293 extract. The precipitates were analyzed by SDS-PAGE and Western blotting with anti-Cherry antibody. Lynx1 interacts with extracellular domains of muscle nAChR subunits (B). Arrows indicate the GST-nAChR fusion proteins and GST (control). Some truncation products containing GST were also detected. Based on the migration pattern, these additional bands likely represent the GST tag that was cleaved of the recombinant proteins. The GST-tagged extracellular domain of nAChRα subunit (nAChRα-GST) was analyzed for its ability to co-precipitate the purified GST-tagged Lynx1 (Lynx1-GST). The pull-down was performed with BTX-biotin attached to the Streptavidin Dynabeads, and the blot was probed with anti-GST antibody. Lynx1-GST co-precipitates with nAChRα-GST (C). The purified extracellular domains of each nAChR subunit (α, β, δ, ε and γ) were analyzed for their ability to pull-down the purified Lynx1-6XHis; GST was used as control (D). The precipitates were analyzed by SDS-PAGE and Western blotting with anti-His and anti-GST antibodies. Lynx1 interacts with extracellular domains of all muscle nAChR subunits. IP, immunoprecipitation.

Figure 3.

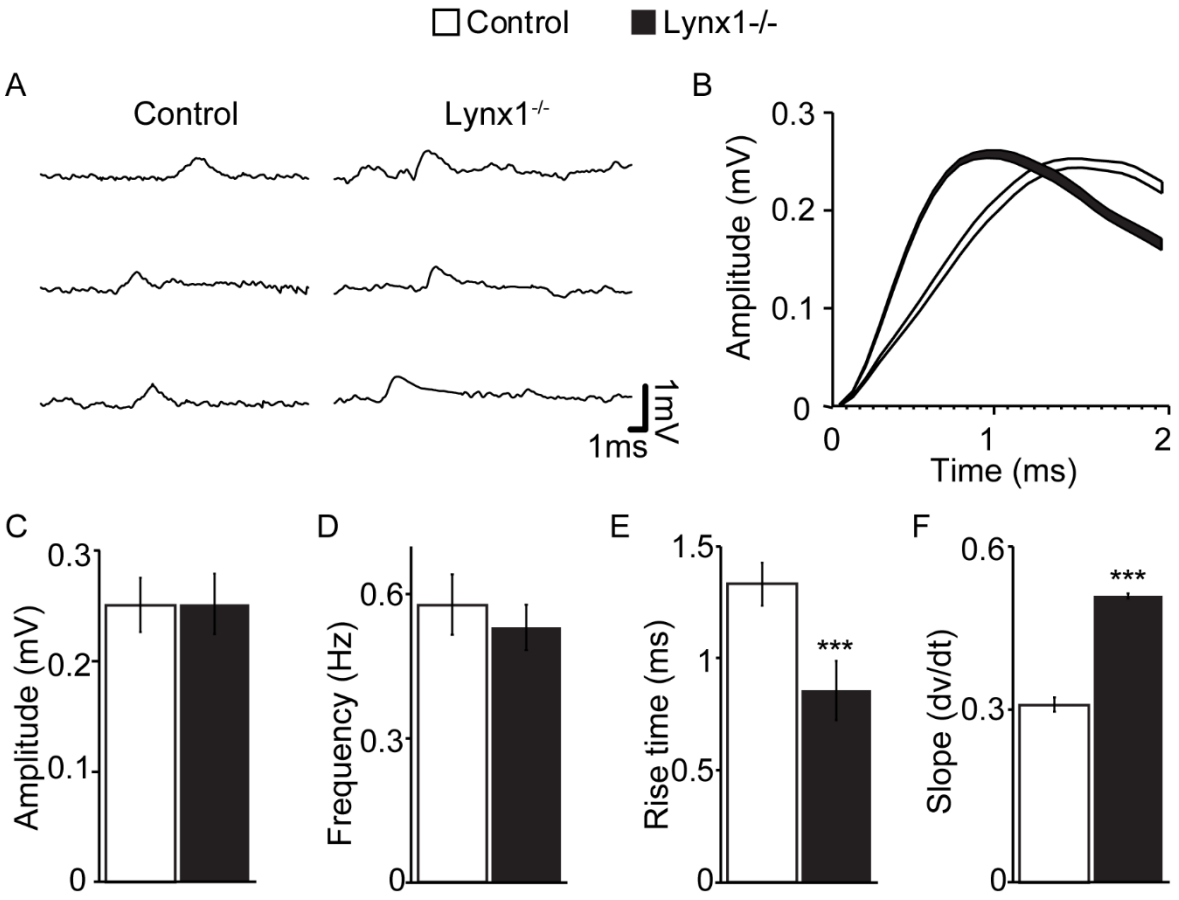

Figure 3. Increased sensitivity in nAChRs lacking Lynx1. Example traces of spontaneous MEPP recordings from control and Lynx1$^{-/-}$ mice (A). An average of 100 traces from control and Lynx1$^{-/-}$ MEPP recordings, where the line width represents SEM (B). The mean amplitude (C) and frequency (D) of MEPPs. The average MEPP rise time to peak amplitude (E) and the slope of MEPPs to peak amplitude (F) between control and Lynx1$^{-/-}$ mice. Data represented as means ± SEM. All male mice were used for this study. Control n=≥ 5, Lynx1$^{-/-}$ n=≥ 8. Statistical significance was determined with unpaired and two-sided Student's t-tests. ***p<0.001.

Figure 4.

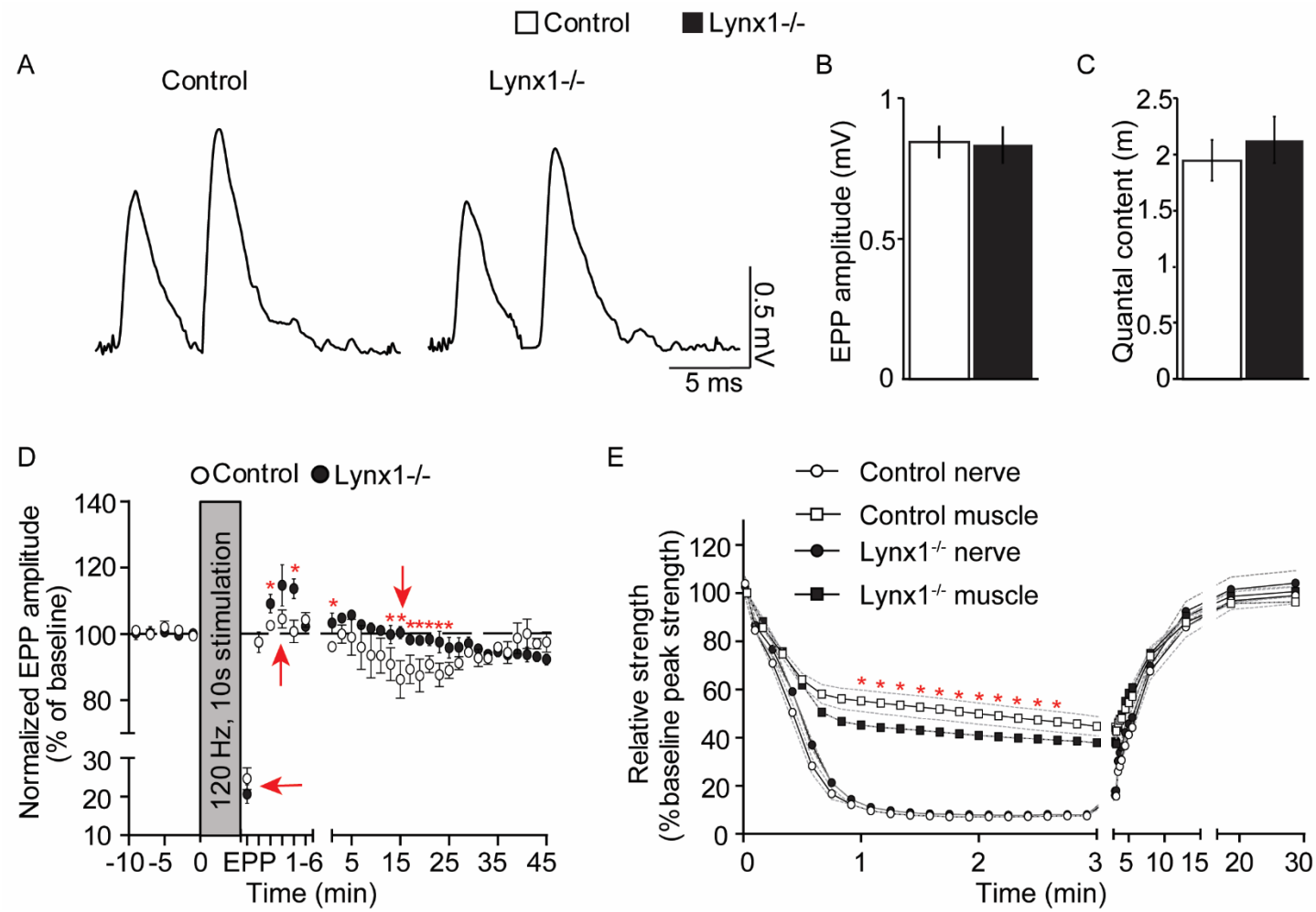

Figure 4. Lynx1 reduces synaptic plasticity and muscle force. Example of recordings of EPPs elicited by paired-pulse stimulation (0.2 Hz, 10 ms interval) from control and Lynx1$^{-/-}$ mice (A), the average EPP amplitude (measured of the first EPP of the pair) (B) and the average quantal content (C). Synaptic plasticity represented as amplitude of EPPs at baseline and following tetanic stimulation, arrows represent significant events (D). Neuromuscular fatigue represented as relative strength from baseline following super-imposed muscle and nerve stimulations after fatigue protocol (E). Data represented as means ± SEM. All male mice were used for this study. Control n=≥ 5, Lynx1$^{-/-}$ n=≥ 8. Statistical significance was determined with unpaired and two-sided Student's t-tests at each time point. *p<0.05.

Figure 5.

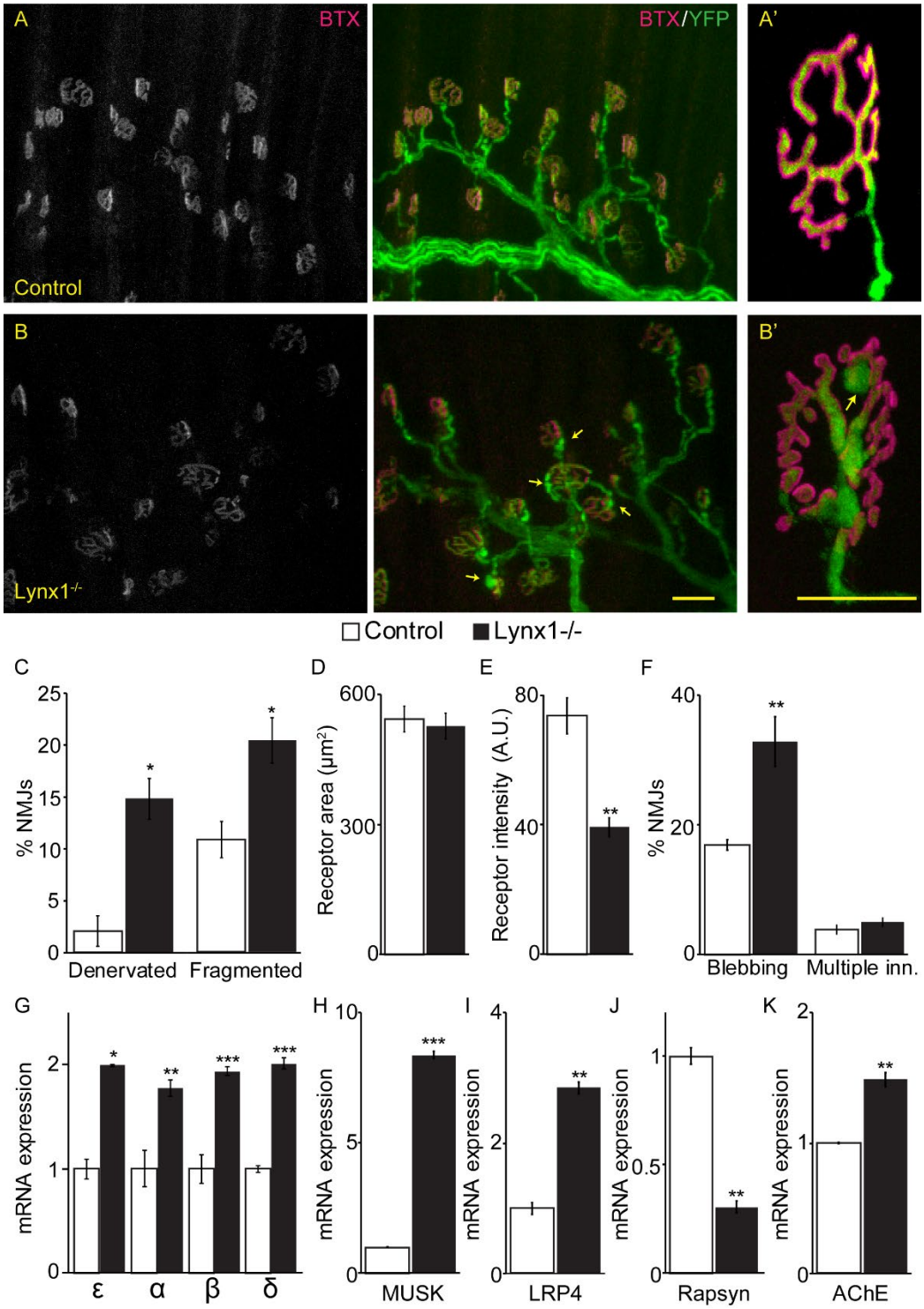

Figure 5. Lynx1 plays a role in NMJ maturation. Analysis of 4-month-old control (A) and Lynx1$^{-/-}$ (B) EDL muscles expressing YFP (green) in nerve endings and nAChRs visualized using BTX (red) shows increased NMJ denervation and fragmentation (B'; C) in Lynx1$^{-/-}$ muscles. The receptor area (D) is unaffected by Lynx1 deletion, but there is a significant decrease in receptor staining intensity (E) in Lynx1$^{-/-}$ mice. There are more blebs on innervating nerves (arrows), with no change in the incidence of multiple innervated nAChRs (F). However, qPCR analysis of 4-month-old TA muscle shows expression of all subunits in the mature muscle nAChR is significantly increased in Lynx1$^{-/-}$ muscles (G). Similarly, MuSK (H) and LRP4 (I) expression are significantly upregulated, while expression of Rapsyn (J) is significantly decreased in Lynx1$^{-/-}$ muscle. Expression of AChE is significantly increased in Lynx1$^{-/-}$ muscles (K). Data represented as means ± SEM. Expression is normalized to GAPDH and relative to control. All male mice were used for this study. Control n=4, Lynx1$^{-/-}$ n=5. At least 30 NMJs were analyzed per animal. Scale Bars=30μm. Statistical significance was determined with unpaired and two-sided Student's t-tests. *P<0.05, **P<0.01, ***P<0.001.

Figure 6.

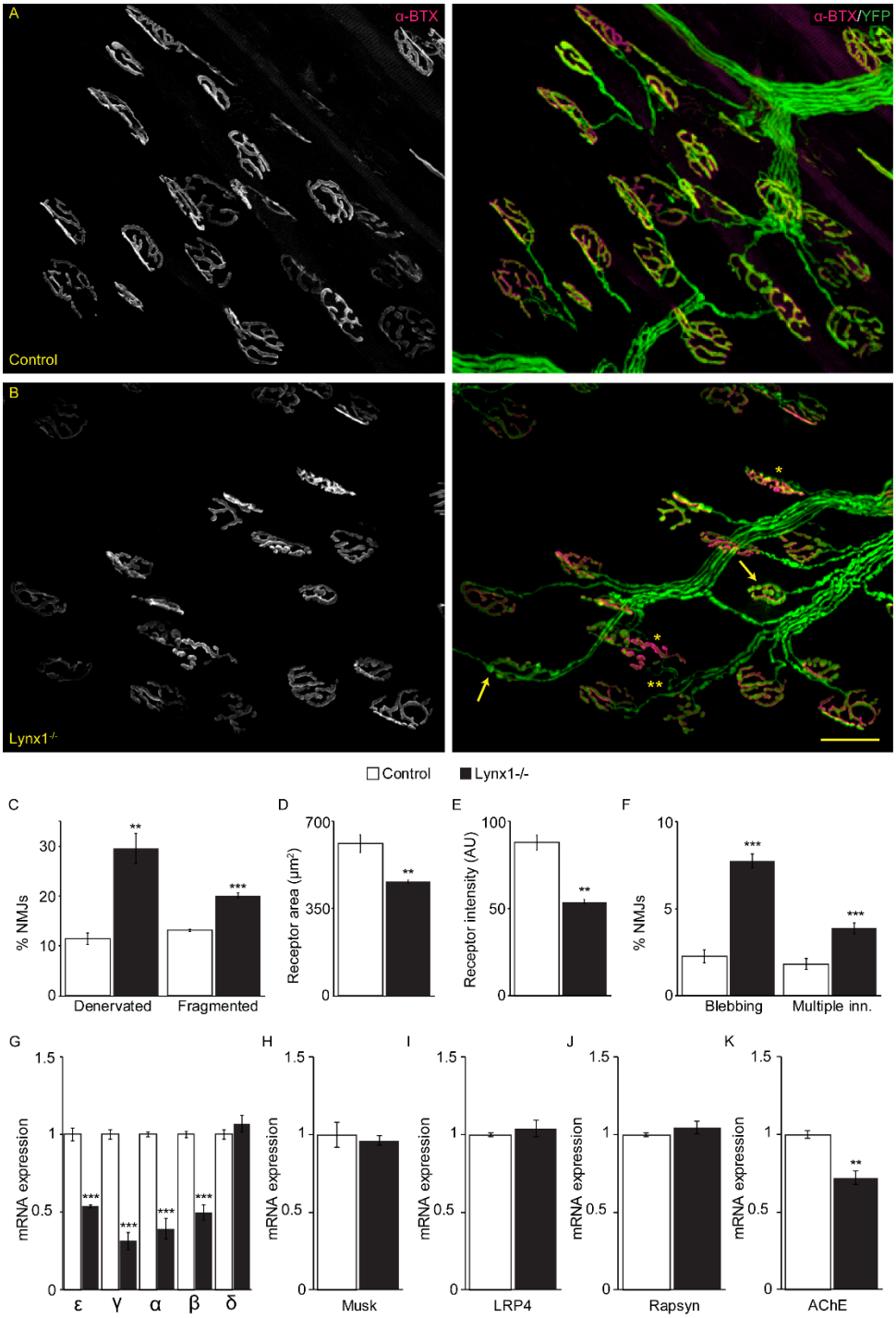

Figure 6. Lynx1 plays a role in NMJ maintenance. Analysis of 12-month-old control (A) and Lynx1$^{-/-}$ (B) EDL muscles expressing YFP (green) in nerve endings and nAChRs visualized using BTX (red) shows increased NMJ denervation and fragmentation in Lynx1$^{-/-}$ muscles (C; *). The area (D) and intensity (E) of nAChRs are also significantly reduced in Lynx1$^{-/-}$ muscles. Furthermore, there is an increase in the incidence of blebbing (arrows) on the innervating nerve and multiple innervated nAChRs (F; **). Expression of ε, γ, α, and β subunits is significantly reduced in Lynx1$^{-/-}$ TA muscles compared to controls (G). While the expression of MuSK (H), LRP4 (I), and Rapsyn (J) are unchanged. expression of AChE is reduced in Lynx1$^{-/-}$ TA muscles (K). Data represented as means ± SEM. Expression is normalized to GAPDH and relative to control. All male mice were used for this study. Control n=4, Lynx1$^{-/-}$ n=4. At least 30 NMJs were analyzed per animal. Scale Bar=30μm. Statistical significance was determined with unpaired and two-sided Student's t-tests. *P<0.05, **P<0.01, ***P<0.001.

Figure 7.

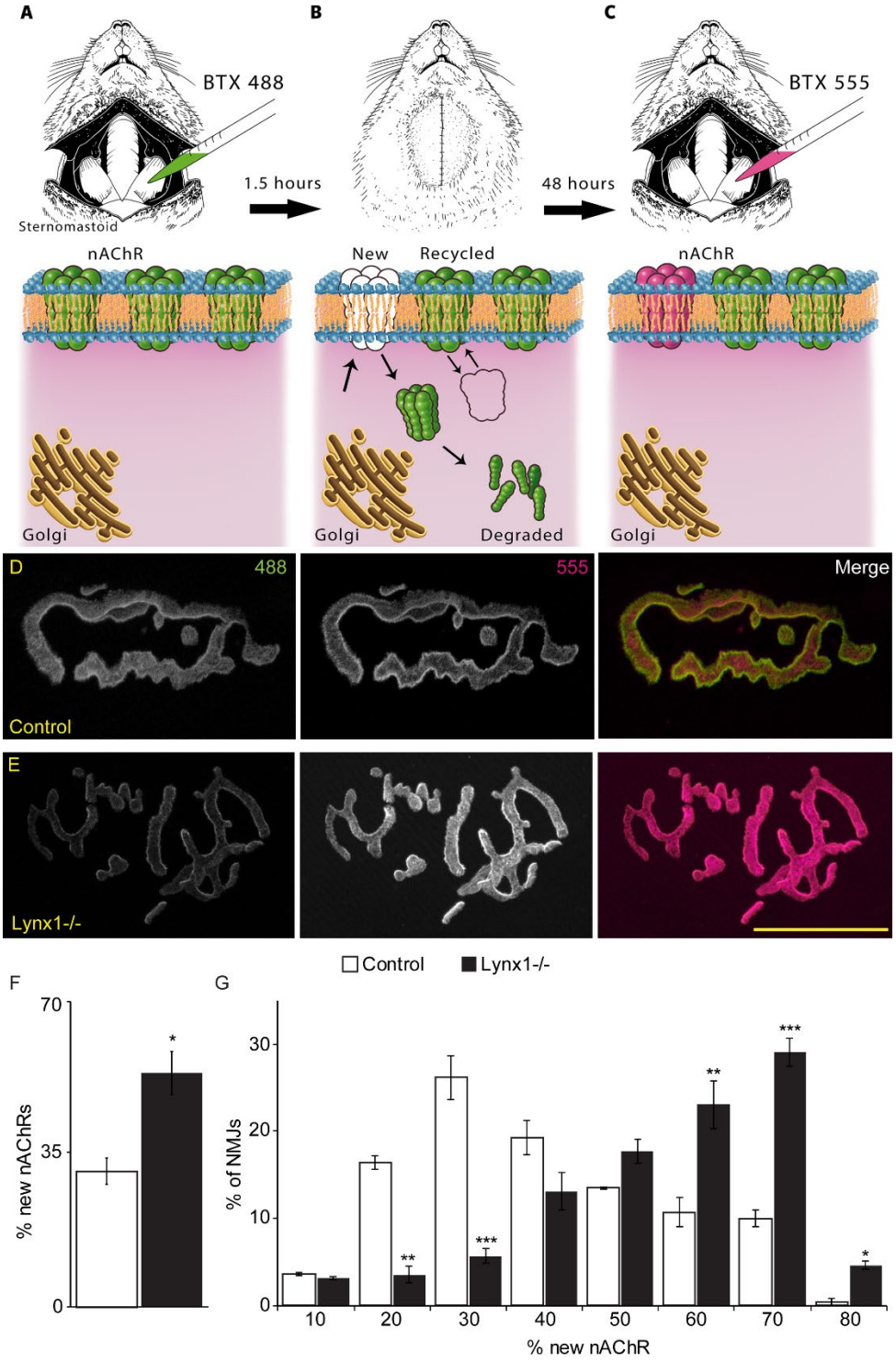

Figure 7. Loss of Lynx1 accelerates nAChR turnover in skeletal muscle. Sternomastoid muscles of 4-month-old mice were surgically exposed and bathed in saturating levels of BTX-488 (green) for 1.5 hours (A), then washed and sutured (B). After 48 hours, sternomastoid muscles were re-exposed and bathed in saturating levels of BTX-555 (red) for 1.5 hours (C). The ratio of intensity between BTX-488 and BTX-555 was determined in control (D) and Lynx1$^{-/-}$ (E) muscles. Lynx1$^{-/-}$ muscles have an increased percentage of newly labeled nAChRs (F). However, there is also substantial variability in nAChR turnover based on individual functional demands and morphological makeup of NMJs within the same muscles. The frequency distribution also shows an increase in the frequency of new nAChRs among NMJs in Lynx1$^{-/-}$ muscles (G). Data represented as means ± SEM. All male mice were used for this study. Control n=4, Lynx1$^{-/-}$ n=4. At least 50 NMJs were analyzed per animal. Scale Bar=30 µm. Statistical significance was determined with unpaired and two-sided Student's t-tests. *P<0.05, **P<0.01, ***P<0.001.

Figure 8.

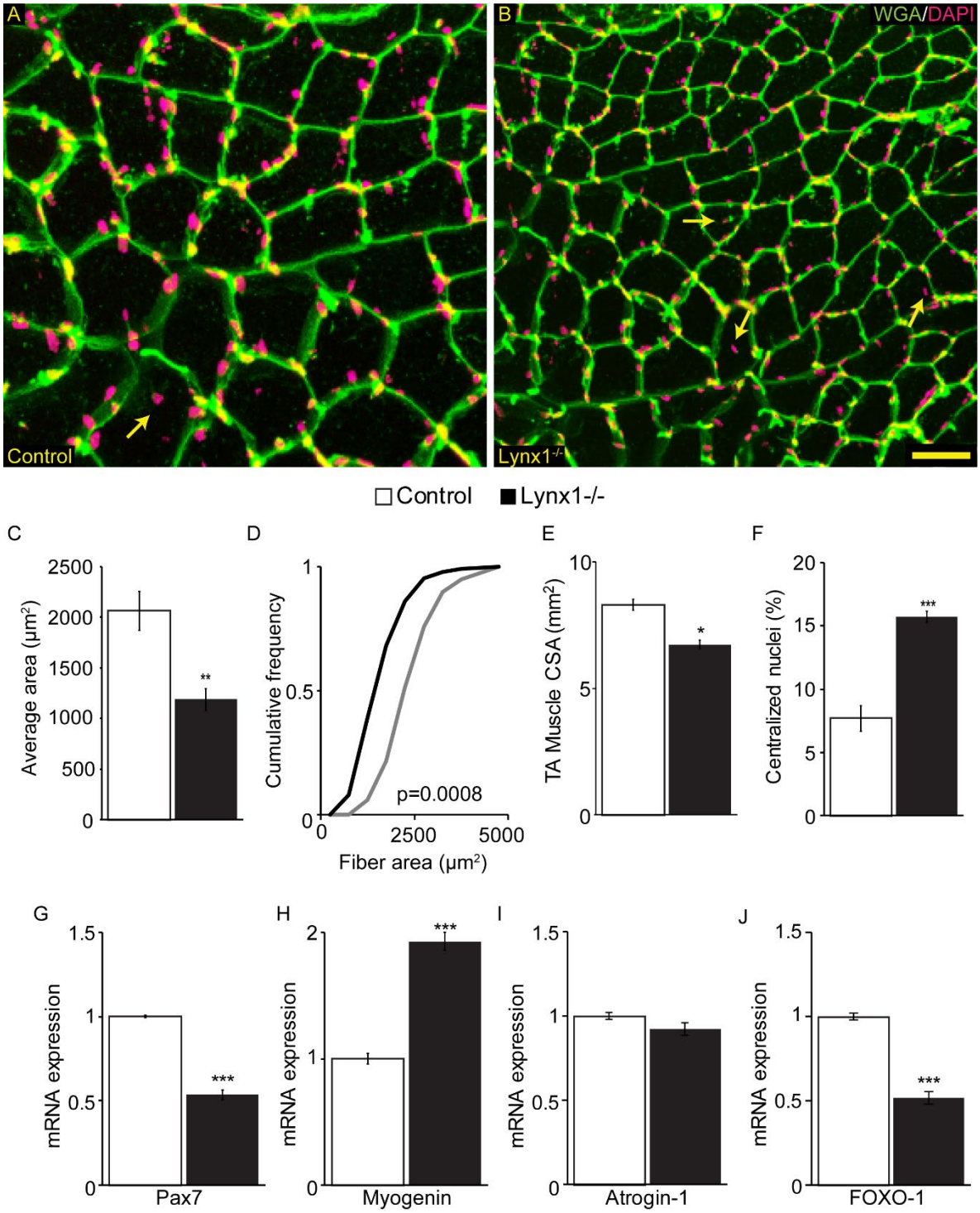

Figure 8. Muscle atrophy in aged Lynx1$^{-/-}$ mice. TA muscles from 12-month-old control (A) and Lynx1$^{-/-}$ (B) mice were cross-sectioned and stained with WGA (green) and DAPI (red) to visualize muscle fibers and their nuclei. Lynx1$^{-/-}$ muscles have a significantly decreased average cross-sectional area compared to controls (C). Similarly, the cumulative frequency distribution of cross-sectional area shows a significant reduction in Lynx1$^{-/-}$ muscles (D). The overall TA muscle CSA is also reduced in Lynx1$^{-/-}$ mice (E). Furthermore, Lynx1$^{-/-}$ muscles have an increase in the incidence of centralized nuclei compared to control muscles (F). Additionally, the mRNA expression of Pax7 is significantly reduced in Lynx1$^{-/-}$ muscles compared to controls (G). In contrast, myogenin expression is considerably increased (H), Atrogin-1 expression is unchanged (I), and FOXO-1 (J) expression is significantly reduced in Lynx1$^{-/-}$ muscles compared to controls. Data represented as means ± SEM. Expression is normalized to GAPDH and relative to control. All male mice were used for this study. Control n=4, Lynx1$^{-/-}$ n=4. At least 100 muscle fibers were analyzed per animal. Scale Bar=30μm. Statistical significance was determined with unpaired and two-sided Student's t-tests and Kolmogorov–Smirnov test (D). *P<0.05, **P<0.01, ***P<0.001.

Figure 9.

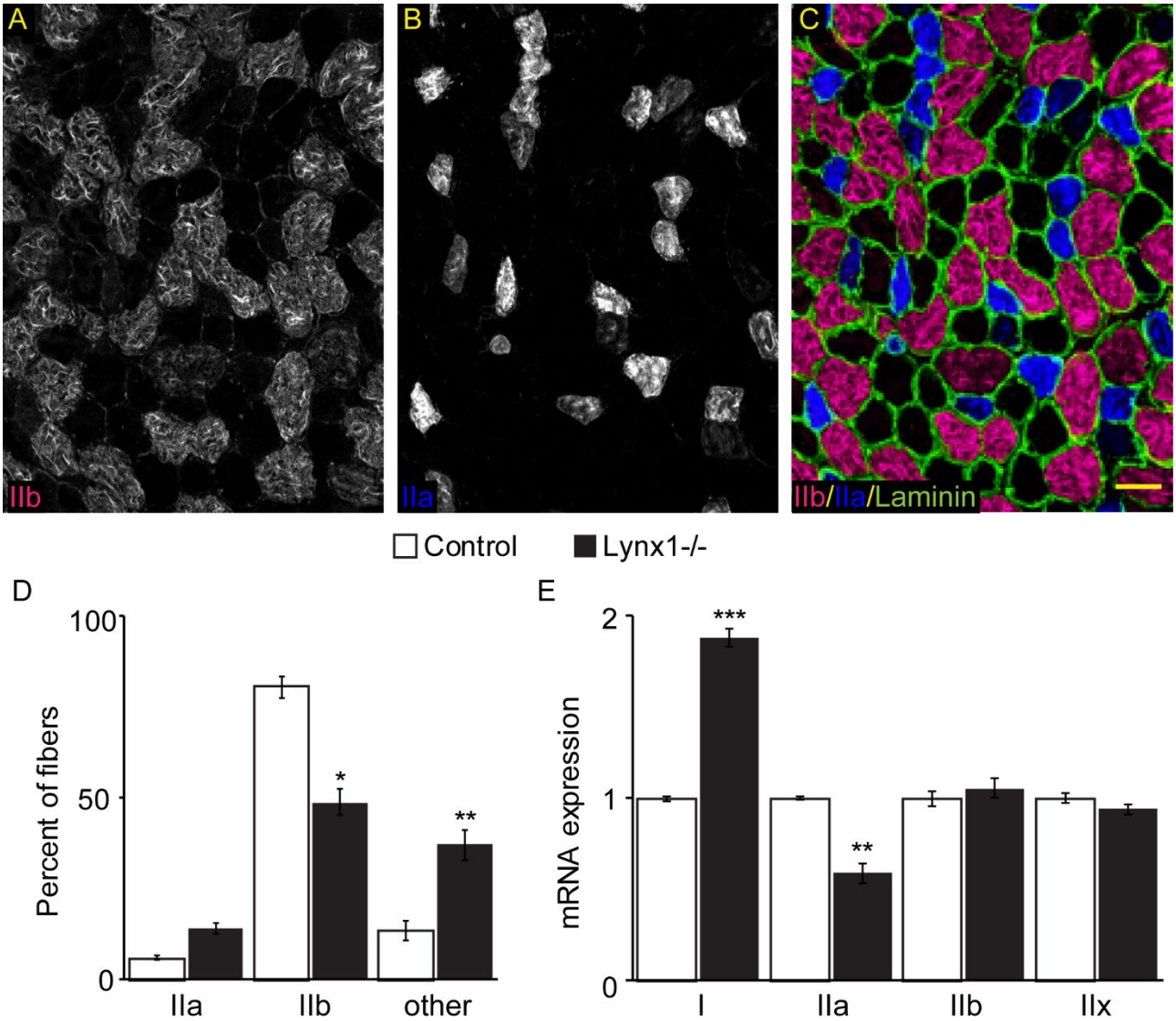

Figure 9. Fiber type shifts in aged Lynx1$^{-/-}$ muscles. TA muscles from 12-month-old control and Lynx1$^{-/-}$ mice were cross sectioned and stained with antibodies against MyHCIIb (A; red), MyHCIIa (B; blue), and laminin (C; green) to examine muscle fiber types. IHC analysis revealed a significant reduction in MyHCIIb fibers, and an increase in fibers that are either MyHCI or MyHCIIx in Lynx1$^{-/-}$ muscles (D). Further analysis of mRNA expression revealed a significant increase in MyHCI, and a reduction in MyHCIIa in Lynx1$^{-/-}$ muscles compared to controls (E). Data represented as means ± SEM. Expression is normalized to GAPDH and relative to control. All male mice were used for this study. Control n=4, Lynx1$^{-/-}$ n=4. At least 100 muscle fibers were analyzed per animal. Scale Bar=30µm. Statistical significance was determined with unpaired and two-sided Student's t-tests. *P<0.05, **P<0.01, ***P<0.001.

Figure 10.

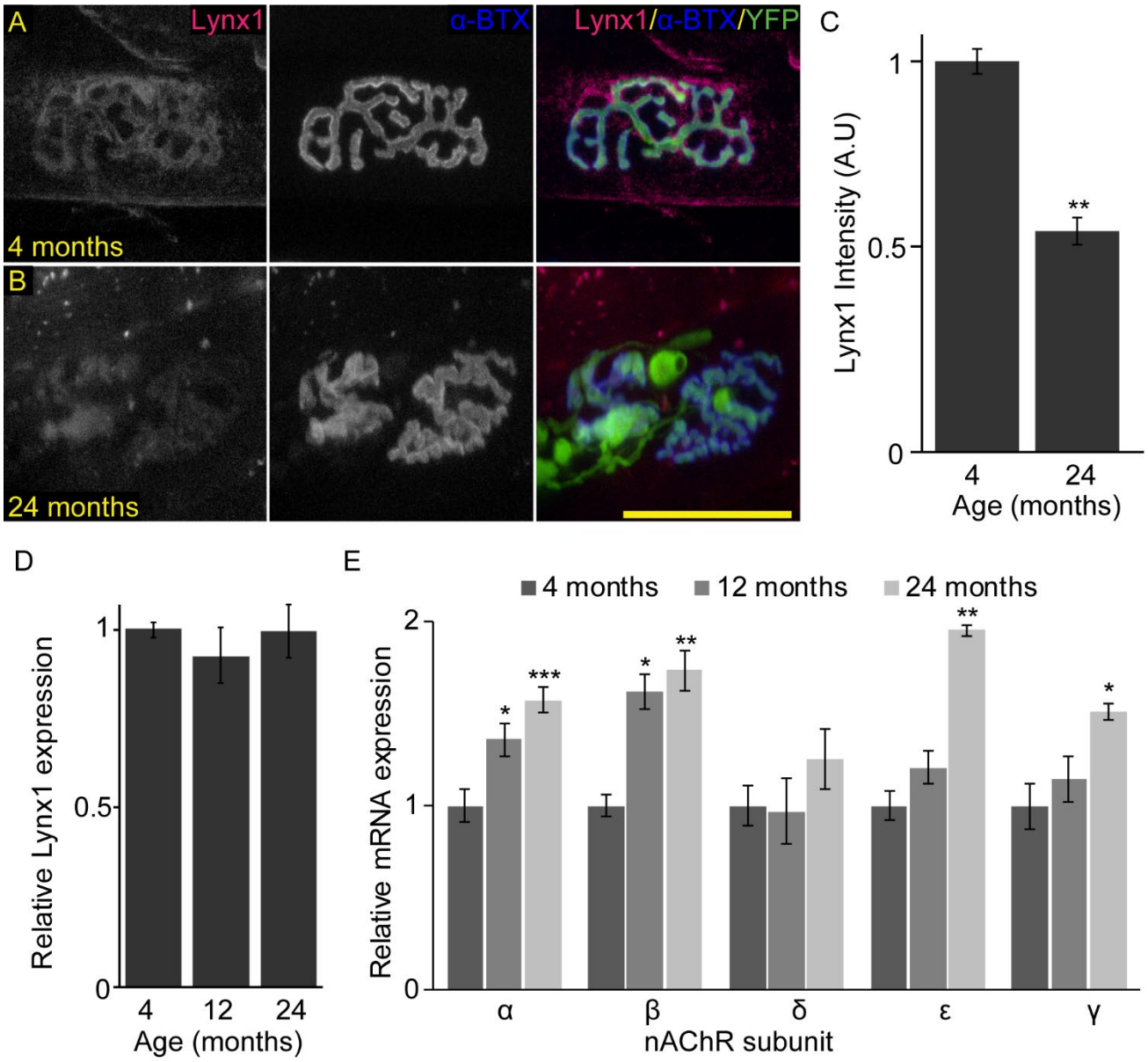

Figure 10. Endogenous Lynx1 expression in aging NMJs. Immunohistochemistry with anti-Lynx1 (red), BTX (blue), and YFP (green) revealed a loss of Lynx1 protein concentrated at the NMJ between 4 months (A) and 24 months of age (B, C). However, expression of Lynx1 remains constant in TA muscles from 4, 12, and 24 month-old animals (D). Expression of nAChR subunits (α, β, ε, and γ) is significantly increased in 24-month-old animals (E). Data represented as means ± SEM. Expression is normalized to GAPDH and relative to 4 months. All male mice were used for this study. 4 months; n=5, 12 months; n=5, 24 months; n=5. Scale Bar=30μm. Statistical significance was determined with unpaired and two-sided Student's t-tests. *P<0.05, **P<0.01, ***P<0.001.

Supplementary Figure 1.

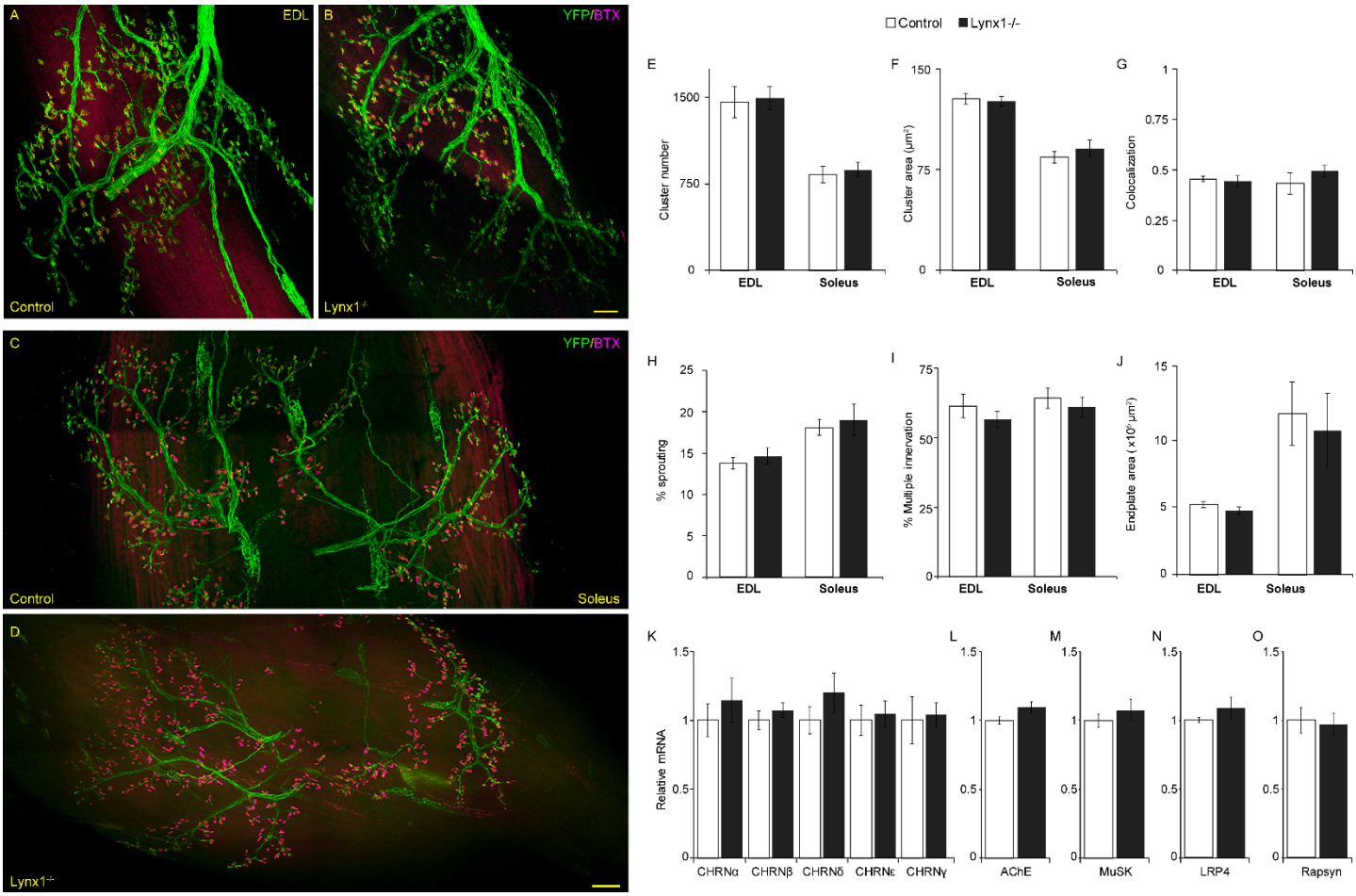

Supplementary Figure 1. Loss of Lynx1 has no discernable impact on NMJ development. The EDL (A,B) and soleus (C,D) muscles were examined from P6 control (A,C) and Lynx1$^{-/-}$ (B,D) mice expressing YFP (green) in nerve endings and nAChRs visualized using BTX (magenta). In both EDL and soleus muscles there are no differences in the number of nAChR plaques (E), the area of nAChR clusters (F), colocalization between YFP and BTX (G), sprouting of the nerve terminal (H), multiply innervated nAChR plaques (I), or the area of the endplate region (J) between control and Lynx1$^{-/-}$ muscles. Similarly, the mRNA expression of nAChR subunits (K), AChE (L), MuSK (M), LRP4 (N), or Rapsyn (O), are unchanged in Lynx1$^{-/-}$ TA muscles compared to controls. Data represented as mean ± SEM. Expression is normalized to GAPDH and relative to control. All male mice were used for this study. Control n = 5, Lynx1$^{-/-}$ n = 6. At least 50 NMJs were analyzed per animal. Scale bar = 20 µm.

Supplementary Figure 2.

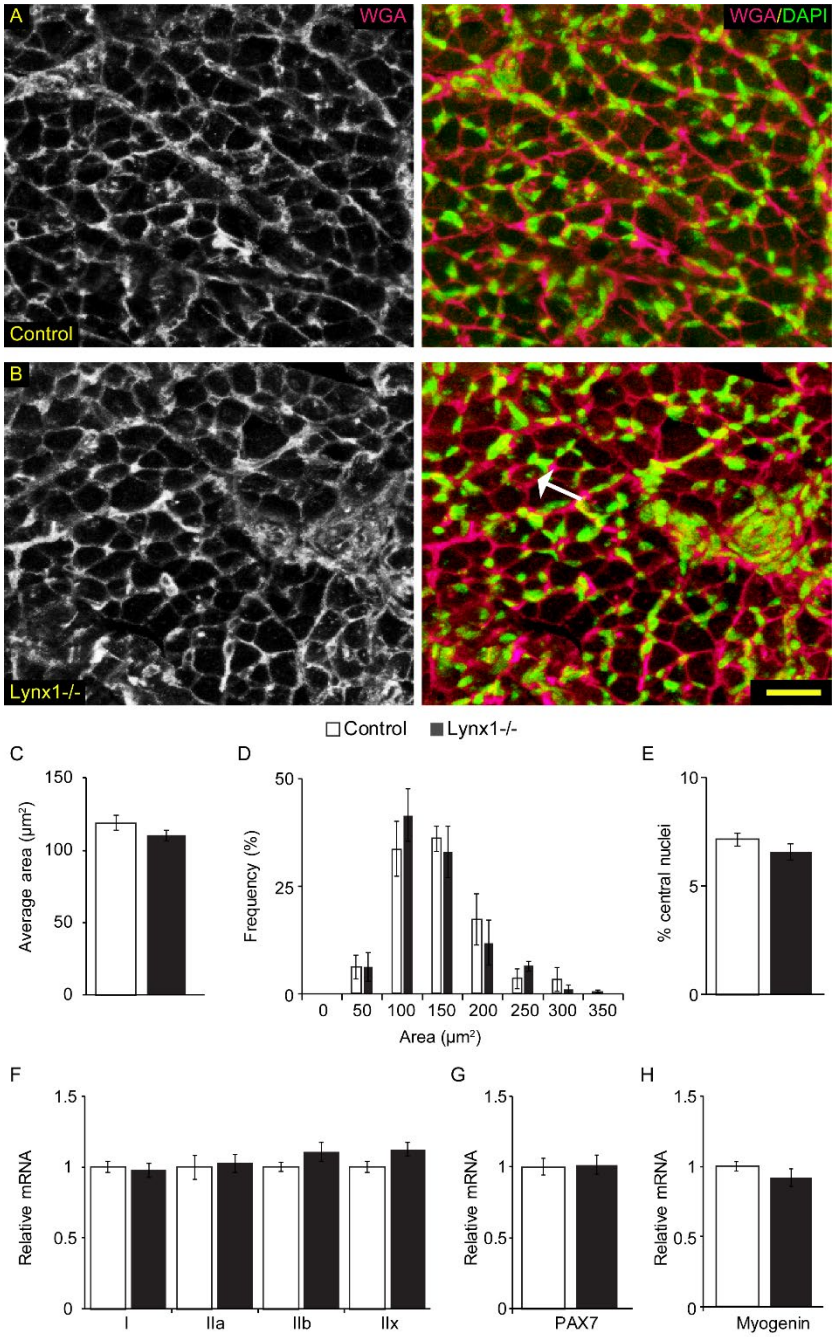

Supplementary Figure 2. Loss of Lynx1 has no effect on muscle fiber development. TA muscles from P6 control (A) and Lynx1$^{-/-}$ (B) mice were cross-sectioned and stained with WGA (magenta) and DAPI (green) to visualize muscle fibers and their nuclei. There is no difference in the average cross-sectional area of muscle fibers from control and Lynx1$^{-/-}$ muscles (C). Similarly, the frequency distribution of cross-sectional area is the same in control and Lynx1$^{-/-}$ muscles (D). There is also no difference in the incidence of centralized nuclei (white arrow) in control and Lynx1$^{-/-}$ muscles (E). Furthermore, the mRNA expression of myosin heavy chains is similar between Lynx1$^{-/-}$ muscles (F). The mRNA expression of Pax7 (G) and myogenin (H) is unchanged in Lynx1$^{-/-}$ TA muscles compared to controls. Data represented as mean ± SEM. Expression is normalized to GAPDH and relative to control. All male mice were used for this study. Control n = 5, Lynx1$^{-/-}$ n = 6. At least 100 muscle fibers were analyzed per animal. Scale bar = 20 μm.

Supplementary Figure 3.

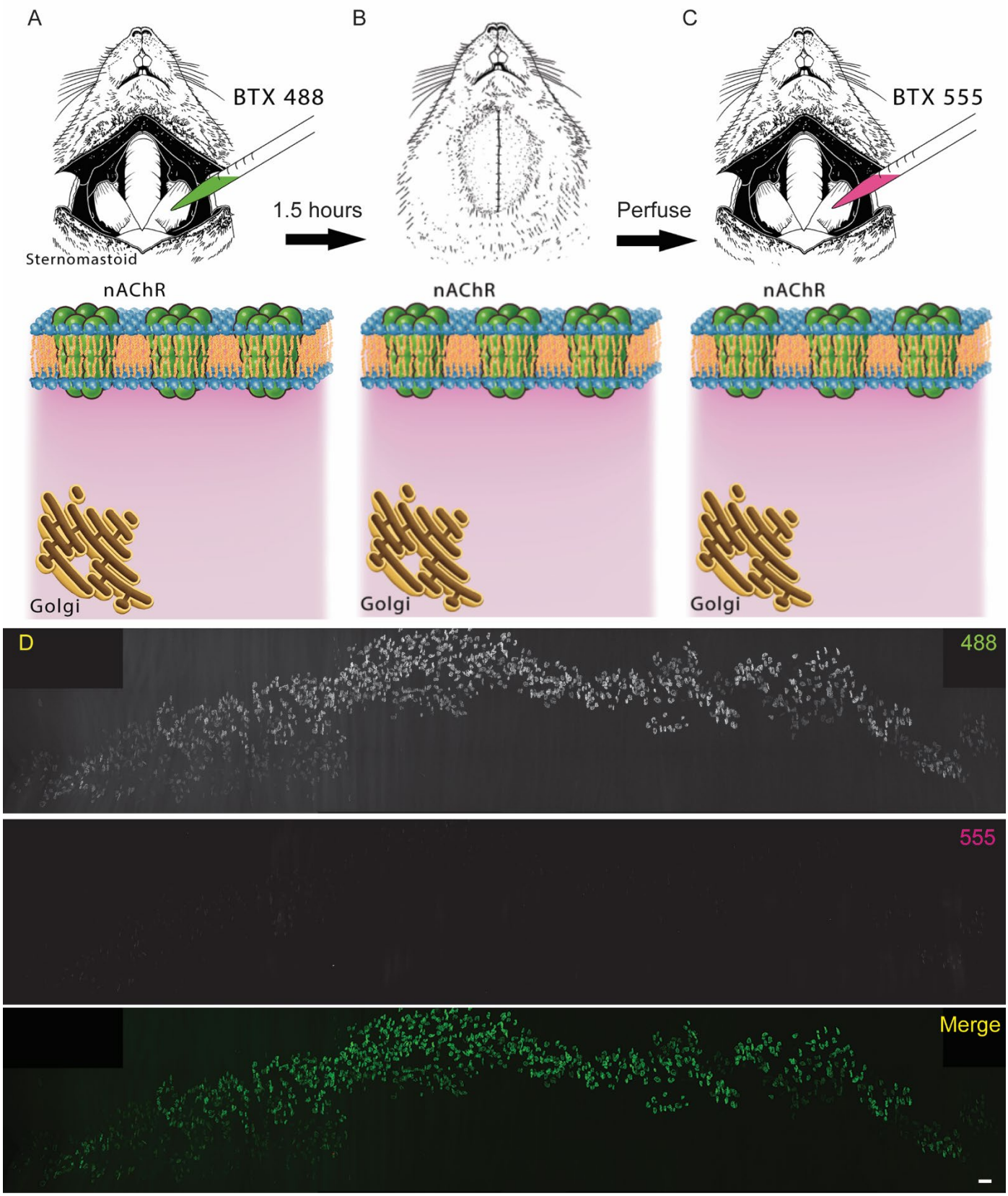

Supplementary Figure 3. nAChR saturation following BTX exposure. Sternomastoid muscles of 4 month-old mice were surgically exposed and bathed in saturating levels of BTX-488 (green) for 1.5 hours (A), then washed and immediately perfused (B). Sternomastoid muscles were subsequently bathed in saturating levels of BTX-555 (red) for 1.5 hours and then imaged (C). nAChRs are saturated by BTX-488, and are unlabeled by BTX-555 (D). Scale Bar=100μm.

Supplementary Figure 4.

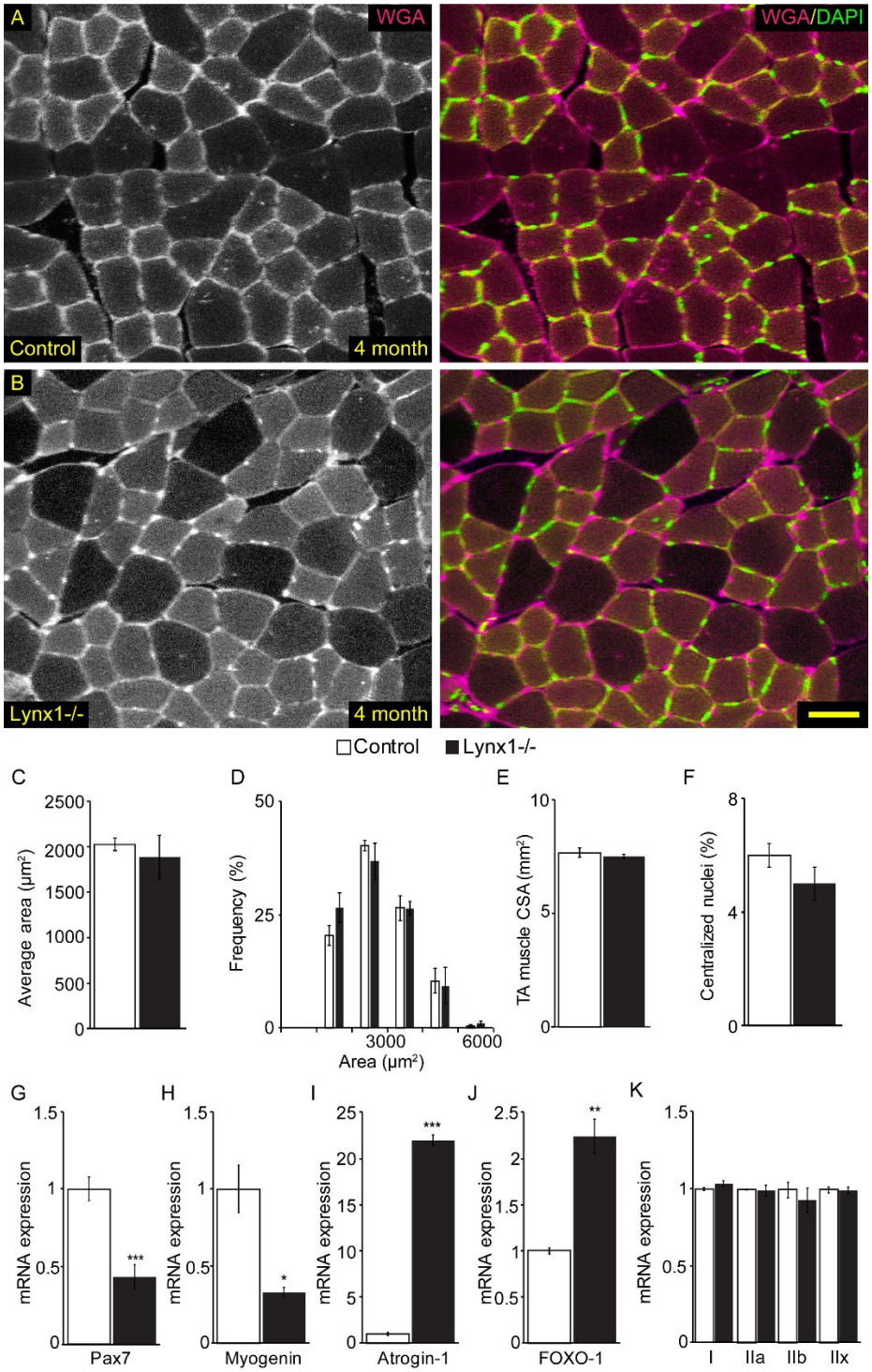

Supplementary Figure 4. Loss of Lynx1 increases signs of atrophy in adult muscle. TA muscles from 4 month-old control (A) and Lynx1$^{-/-}$ (B) mice were cross-sectioned and stained with WGA (magenta) and DAPI (green) to visualize muscle fibers and their nuclei. There is no difference in the average cross-sectional area of muscle fibers from control and Lynx1$^{-/-}$ muscles (C). Similarly, the frequency distribution of cross-sectional area is the same in control and Lynx1$^{-/-}$ muscles (D). Furthermore, there is no difference in the whole muscle CSA between control and Lynx1$^{-/-}$ TA muscles (E). There is also no difference in the incidence of centralized nuclei in control and Lynx1$^{-/-}$ muscles (F). However, the mRNA expression of Pax7 (G) and myogenin (H) is significantly reduced in Lynx1$^{-/-}$ muscles compared to controls. In contrast, Atrogin-1 (I) and FOXO-1 (J) expression is substantially increased in Lynx1$^{-/-}$ muscles compared to controls. However, the mRNA expression of myosin heavy chains is similar between Lynx1$^{-/-}$ muscles (K). Data represented as mean ± SEM. Expression is normalized to GAPDH and relative to control. All male mice were used for this study. Control n=4, Lynx1$^{-/-}$ n=4. At least 100 muscle fibers were analyzed per animal. Scale Bar=30μm. *P<0.05, **P<0.01, ***P<0.001.

Supplementary Figure 5.

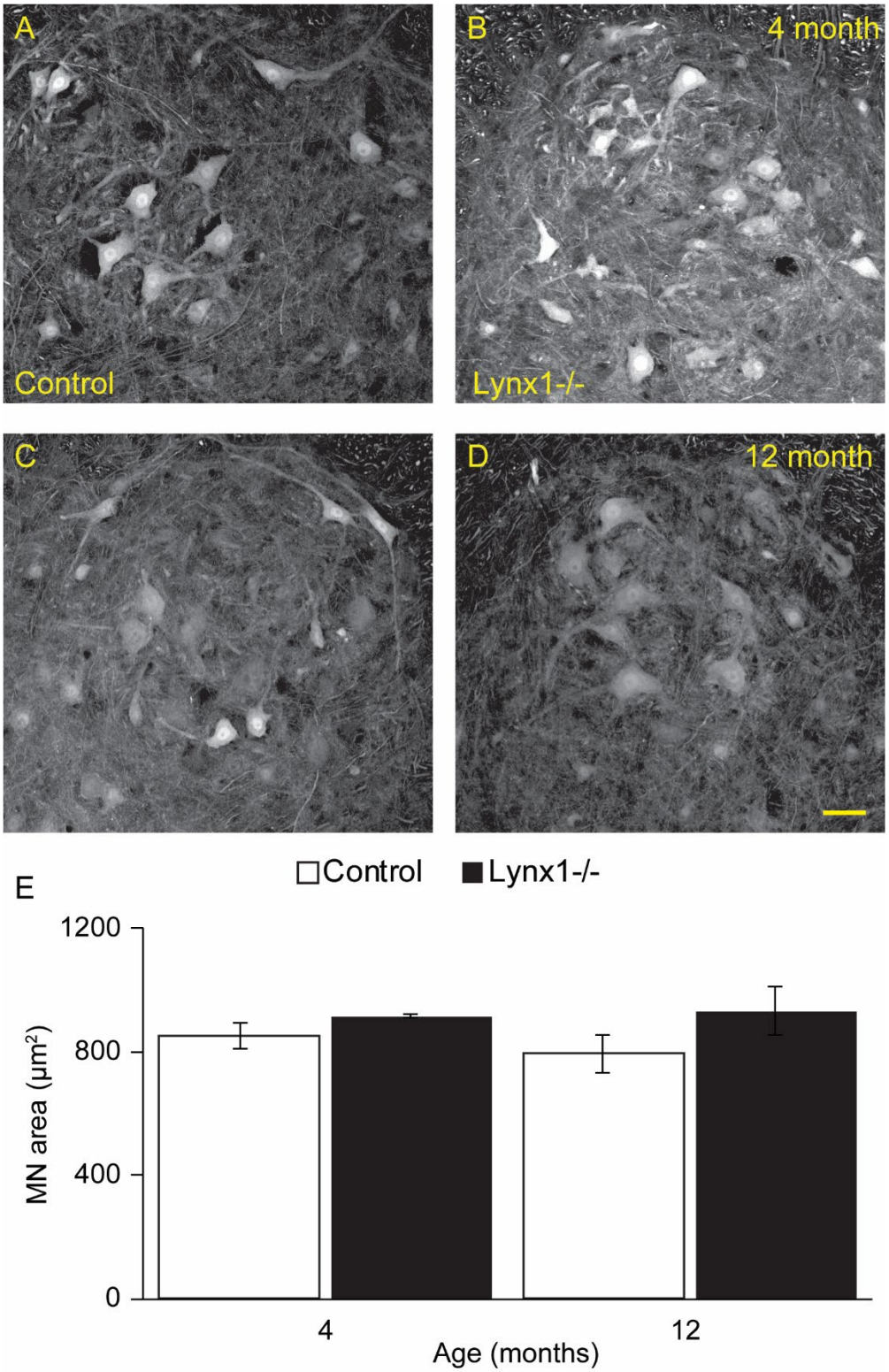

Supplementary Figure 5. No changes in motor neurons from Lynx1$^{-/-}$ mice.
Spinal cords from 4 month-old control (A) and Lynx1$^{-/-}$ (B) and 12 month-old control (C) and Lynx1$^{-/-}$ (D) mice were cross-sectioned. Motor neurons in the ventral horn were visualized using transgenic YFP expression. There is no difference in the average motor neuron area from control and Lynx1$^{-/-}$ spinal cords at 4 or 12 months of age (E). Data represented as mean ± SEM. All male mice were used for this study. Control n=4, Lynx1$^{-/-}$ n=4. At least 20 motor neurons were analyzed per animal. Scale Bar=50μm.

Table 1. qPCR primers

Gene	Fw (5'-3')	Rv (5'-3')
AChE	CTACACCACGGAGGAGAGGA	CTGGTTCTTCCAGTGCACCA
Atrogin-1	GCAGCAGCTGAATAGCATCCA	GGTGATCGTGAGGCCTTTGAA
CHRNα	CTTCAAAGAGCTTTGCCACC	CCATGGAGCTCTCGACTGTT
CHRNβ	AGGTCTCAGGCACTTTGTCG	TTCTACCTCCCACCAGATGC
CHRNδ	CCGATGCACTATCTCCCACT	CTTAGCCTGAAGCAGGAGGA
CHRNε	GCTGTGTGGATGCTGTGAAC	GCTGCCCAAAAACAGACATT
CHRNγ	GCTCAGCTGCAAGTTGATCTC	CCTCCTGCTCCATCTCTGTC
FOXO-1	GAGTTAGTGAGCAGGCTACATTT	TTGGACTGCTCCTCAGTTCC
GAPDH	CCCACTCTTCCACCTTCGATG	GTCCACCACCCTGTTGCTGTAG
LRP4	GGCAAAAAGCAGGAACTTGT	TCTACCCAGTGGCCAGAACT
Lynx1	ACCACTCGAACTTACTTCACC	ATCGTACACGGTCTCAAAGC
MUSK	CCGATGTGTCTGCTCTTTGA	ACAGGACAGTGGTGGAGGAC
Myogenin	ACCAGGAGCCCCACTTCTAT	GTCCCCAGTCCCTTTTCTTC
MyHCI	CTCAAGCTGCTCAGCAATCTATTT	GGAGCGCAAGTTTGTCATAAGT
MyHCIIa	GAGTGAGCAGAAGCGGAATGCT	GCGGAACTTGGATAGATTTGTG
MyHCIIb	CACCTGGACGATGCTCTCAGA	GCTCTTGCTCGGCCACTCT
MyHCIIx	GCTAGTAACATGGAGGTCA	TAAGGCACTCTTGGCCTTTATC
Pax7	GCGAGAAGAAAGCCAAACAC	GTCGGGTTCTGATTCCACAT
Rapsyn	GTGCCATGGAGTGTTGTGAG	CGGTTTCCGATCTCAGTCAT